A NONLINEAR REDUCED ORDER METHOD FOR PREDICTION OF ACOUSTIC FATIGUE

Adam Przekop*
Staff Scientist
National Institute of Aerospace
Hampton, VA 23666-1339

Stephen A. Rizzi
Aerospace Engineer
NASA Langley Research Center
Structural Acoustics Branch
Hampton, VA 23681-2199

Number of Pages: 52
Number of Figures: 21
Number of Tables: 4

* ALL CORRESPONDENCE SHOULD BE DIRECTED TO:

Adam Przekop
National Institute of Aerospace
c/o NASA Langley Research Center
Structural Acoustics Branch
Mail Stop 463
Hampton, VA 23681-2199

Phone: 757-864-2278
Fax: 757-864-8823
Email: fn.a.przekop@larc.nasa.gov

A NONLINEAR REDUCED ORDER METHOD FOR PREDICTION OF ACOUSTIC FATIGUE

ABSTRACT

The goal of this investigation is to assess the quality of high-cycle-fatigue life estimation via a reduced order method, for structures undergoing geometrically nonlinear random vibrations. Modal reduction is performed with several different suites of basis functions. After numerically solving the reduced order system equations of motion, the physical displacement time history is obtained by an inverse transformation and stresses are recovered. Stress ranges obtained through the rainflow counting procedure are used in a linear damage accumulation method to yield fatigue estimates. Fatigue life estimates obtained using various basis functions in the reduced order method are compared with those obtained from numerical simulation in physical degrees-of-freedom.

KEYWORDS

Nonlinear random response, High-cycle-fatigue, Reduced order methods

1. INTRODUCTION

Direct numerical simulation of nonlinear random response in physical degrees-of-freedom (DoFs) is computationally intensive for even the simplest structures. Its use for design of high-cycle-fatigue tolerant aerospace vehicle structures is considered impractical. Accordingly, much effort has been spent in recent years to develop accurate reduced order analyses, which could be suitable for use in design environments.

Finite-element-based nonlinear modal numerical simulation methods have been the focus of much of the research effort as they offer the ability to investigate practical structures. Such methods may be viewed as being in one of two categories; those in which the nonlinear modal stiffness is directly evaluated from the nonlinear finite element stiffness matrix (so-called direct methods), and those in which the nonlinear modal stiffness is indirectly evaluated. Direct methods are typically implemented in special purpose finite element codes in which the nonlinear stiffness is known, see for example references [1-3]. Indirect stiffness evaluation methods are typically implemented for use with commercial finite element codes in which the nonlinear stiffness is unavailable, see for example references [4, 5]. For both direct and indirect stiffness evaluation approaches, the crux of the problem lies in the selection of the proper basis, through which the nonlinear modal stiffness may be determined. Through comparison with numerical simulation in physical DoFs, the authors recently demonstrated [6] the ability of a reduced order method to accurately predict geometrically nonlinear random displacement and stress response, provided that a suitable modal basis is utilized. The focus of this paper is to extend that work to determine the effect of modal basis selection on high-cycle-fatigue life estimation.

The problems of interest are those that exhibit nonlinear bending-membrane coupling. This coupling dramatically changes the stress response characteristics with increasing load, as shown by direct numerical simulation results in Figure 1 to Figure 4 for a clamped-clamped beam under distributed loading. For low-level excitation (128 dB), the total surface stress response has a zero mean component (Figure 1), has a Gaussian probability density function (PDF) distribution and is typically dominated by the bending component (Figure 3). As the excitation level increases, the contribution of membrane stress to the total becomes more significant, resulting in a non-zero mean (Figure 1) which skews the total stress PDF from Gaussian (Figure 2). Additionally for the spring hardening case shown, the stress power spectral density (PSD) exhibits peak broadening and shifting to higher frequencies (Figure 4), and indicates significant peaks due solely to the membrane component. From a mechanics point of view, the reduced order analysis must be capable of accurately predicting all of these behaviors. However, from the fatigue point of view, the *stress range* PDF and stress ratio govern the fatigue life estimate for a given material system. Thus, for fatigue analysis, the reduced order method should be sufficient if it can accurately predict these quantities.

In an effort to determine what selection of basis functions most accurately predicts the stress range PDF and stress ratio, several bases are considered including (i) bending modes only; (ii) coupled bending and companion modes; (iii) uncoupled bending and companion [7, 8] modes; and (iv) bending and membrane modes. Results are compared with those obtained from numerical simulation in physical DoFs. A planar aluminum beam is considered to keep the computational cost of the numerical simulation in physical DoFs reasonable. Two locations along the span of the beam are investigated – one at the clamped end where the bending stress

component is dominant and one at a location close to the quarter-span, where the effect of membrane stress is more significant.

2. NONLINEAR MODAL SIMULATION

The nonlinear modal simulation analysis consists of several parts. The linear system matrices are first obtained from a commercial finite-element program. One or more methods, to be discussed, are next used to obtain a modal basis. Following a transformation of the nonlinear system to modal coordinates, the modal stiffness coefficients are evaluated and the resulting coupled system of equations is numerically integrated to obtain the modal displacement time history. These are transformed back to physical coordinates for post-processing, including stress recovery.

2.1.MODAL COORDINATE TRANSFORMATION

The equations of motion of the nonlinear system in physical degrees-of-freedom may be written as

$$\boldsymbol{M}\ddot{\boldsymbol{X}}(t)+\boldsymbol{C}\dot{\boldsymbol{X}}(t)+\boldsymbol{F}_{\boldsymbol{NL}}(\boldsymbol{X}(t))=\boldsymbol{F}(t). \tag{1}$$

where $\boldsymbol{M}$ and $\boldsymbol{C}$ are the mass and proportional damping matrices, respectively, $\boldsymbol{X}$ and $\boldsymbol{F}$ are the displacement response and force excitation vectors, respectively. The nonlinear restoring force $\boldsymbol{F}_{\boldsymbol{NL}}$ contains the linear, quadratic and cubic stiffness terms.

A set of coupled modal equations with reduced degrees-of-freedom is first obtained by applying the modal coordinate transformation $\boldsymbol{X}=\boldsymbol{\Phi q}$ to Equation (1), where $\boldsymbol{q}$ is the modal displacement response vector. The modal basis function matrix $\boldsymbol{\Phi}$ is typically formed from the eigenvectors obtained from Equation (1) using only the linear stiffness. For flat isotropic structures, these may include any combination of bending and membrane modes. In lieu of

membrane modes, the modal basis may include "companions" related to the membrane response, as discussed in the next section. Generally, a small set of L basis functions are included giving

$$\tilde{\boldsymbol{M}}\ddot{\boldsymbol{q}}(t)+\tilde{\boldsymbol{C}}\dot{\boldsymbol{q}}(t)+\tilde{\boldsymbol{F}}_{\boldsymbol{NL}}(q_1(t),q_2(t),\ldots,q_L(t))=\tilde{\boldsymbol{F}}(t) \tag{2}$$

where the tilde superscript represents modal quantities, and

$$\tilde{\boldsymbol{M}}=\boldsymbol{\Phi}^T\boldsymbol{M}\boldsymbol{\Phi} \qquad \tilde{\boldsymbol{C}}=\boldsymbol{\Phi}^T\boldsymbol{C}\boldsymbol{\Phi}=\lceil 2\zeta_r\omega_r \rfloor \qquad \tilde{\boldsymbol{F}}_{NL}=\boldsymbol{\Phi}^T\boldsymbol{F}_{NL} \qquad \tilde{\boldsymbol{F}}=\boldsymbol{\Phi}^T\boldsymbol{F}\,. \tag{3}$$

2.2. MODAL BASIS CALCULATION

For the problems of interest in this paper, both bending and membrane behavior should be included in the basis selection since the large deflection nonlinearity couples their response. The basis functions may be determined via several methods. Basis functions corresponding to the bending and membrane response may be determined through solution of the linear eigenvalue problem. Other basis functions corresponding to the membrane response induced by bending-membrane coupling may be determined via alternative approaches.

2.2.1. LINEAR EIGENVECTORS

In this study, only isotropic materials or laminated composite materials having zero laminate coupling stiffness ([B]=0) are considered. Further, the current work is restricted to planar structures. The linear eigenvectors obtained from Equation (1) (using only the linear stiffness) are therefore uncoupled and are either associated with low-frequency bending modes or high-frequency membrane modes. The selection of which bending modes to include depends on both the excitation bandwidth and the loading distribution. The identification of each selected bending mode is straightforward as they are typically the lowest frequency modes. The selection of which membrane modes to include is less apparent. All or most membrane modes will likely fall outside the excitation bandwidth. Furthermore, the identification of any particular membrane mode may be difficult and time consuming. Nevertheless, a reasonable starting point

is to select the lowest membrane modes that are consistent with the loading distribution. Inclusion of both these eigenvectors in the modal basis is subsequently referred to as the bending and membrane mode (BM) case. Inclusion of only the bending eigenvectors will be referred to as the bending mode only (B) case. In this study, the mass-normalized linear eigenvectors were obtained using MSC.NASTRAN normal modes analysis (solution 103).

2.2.2. COMPANION BASIS FUNCTIONS

An alternative approach to using membrane modes is the use of so-called companion [7] (or dual [8]) modes. These modes represent the membrane behavior resulting from bending due to bending-membrane coupling. Previous authors utilized quasi-static approaches to determine the companion mode via nonlinear static analyses.

A new method was recently presented for computing the companion mode using a dynamic analysis [6]. An initial stress-free imperfection in the shape of the first bending mode is introduced in the flat structure to couple the bending-membrane response. The magnitude of the imperfection is chosen to be very small such that a normal modes analysis yields virtually the same bending eigenvalues and eigenvectors as that of the flat structure. MSC.NASTRAN solution 103 was again used to compute the mass-normalized eigenvectors, which now contain both the bending and membrane behaviors, but at the natural frequencies of the original flat structure. Direct inclusion of these eigenvectors in the modal basis is subsequently referred to as the coupled bending and companion mode (CBC) case. A more consistent usage relative to the BM basis, however, is to separate the degrees-of-freedom (DoFs) associated with the bending and membrane behaviors. In practice, since the bending behavior is unchanged, the original mass normalized low-frequency bending modes are retained. The bending DoFs are set to zero in the newly obtained eigenvector to obtain the dynamic companion. Inclusion of both these

eigenvectors in the modal basis, independently or in pairs, is subsequently referred to as the uncoupled bending and companion mode (UBC) case. It should be noted that although the CBC basis functions are mass normalized in NASTRAN Solution 103, companions in the UBC set are not. This is because they are obtained through separation of bending and membrane related components from the mass-normalized CBC. Therefore, after separation, they must be again mass-normalized outside the commercial eigen-solver.

2.3. INDIRECT STIFFNESS EVALUATION METHOD

The indirect stiffness evaluation method [5] with a modification that incorporates the linear stiffness in the nonlinear force term [8] was applied. To summarize, the nonlinear force vector in Equation (2) may be written in the form

$$\tilde{F}_{NL}(q_1, q_2, \ldots, q_L) = \sum_{j=1}^{L} d_j^r q_j + \sum_{j=1}^{L}\sum_{k=j}^{L} a_{jk}^r q_j q_k + \sum_{j=1}^{L}\sum_{k=j}^{L}\sum_{l=k}^{L} b_{jkl}^r q_j q_k q_l \qquad r = 1, 2, \ldots, L \tag{4}$$

where d, a, and b are the linear, quadratic nonlinear, and cubic nonlinear modal stiffness coefficients, respectively. This form reduces the problem of determining the nonlinear stiffness from one in which a large set of simultaneous nonlinear equations must be solved to one involving simple algebraic relations. The algebraic relations are obtained by solving a series of nonlinear static problems with prescribed displacement fields.

2.4. NUMERICAL INTEGRATION AND ELEMENT STRESS RECOVERY

Having the nonlinear force vector in Equation (4) fully defined, the coupled modal nonlinear equations of motion in Equation (2) are numerically integrated using a fourth-order Runge-Kutta method [9]. The resulting modal displacement time histories are transformed back to physical coordinates using the inverse modal transformation.

In contrast to mapping techniques relating stress to physical DoFs [7, 8], the approach taken here recovers the element stresses by post-processing the nodal physical DoFs directly within the

finite element program. Since the stress post-processor of the finite element program is used, the stresses are identical to those that would have been obtained via a standard finite element analysis in physical DoFs. The appeal of direct stress recovery over mapping techniques is that it eliminates any issues concerning the accuracy of the mapping, and eliminates the need for estimating nonlinear mapping functions for each stress quantity of interest. The disadvantage is that it can be computationally costly.

In principle, the approach taken is simple. For a single element stress recovery, a finite element mesh is made consisting of two elements; a stress recovery element and a dummy element. The stress recovery element is of the same type and has the same properties as the element of interest. For a particular output time step, the element physical DoFs, obtained via the nonlinear modal simulation method, are applied to each element node as prescribed displacement fields in the MSC.NASTRAN nonlinear static solution. A nuance of MSC.NASTRAN requires the attachment of a dummy element and load [10] to the stress recovery element, in order to calculate the resulting element nodal forces and recover the element stress. By repeating this operation for each output time step, the stress time history is determined. If stress recovery is required for a region or the entire structure, that portion of the original model is used and a dummy element is attached. The prescribed displacement field spans the entire region of interest.

3. FATIGUE LIFE CALCULATION

A comprehensive study of stress range counting methods for fatigue life prediction [11] concluded that the rainflow counting method provides accurate life estimates. This approach is adopted herein. Using this approach, the stress range PDF is obtained from the stress time

history. The fatigue life is estimated using the stress range PDF, appropriate material stress-life (*S*-*N*) data, and a linear cumulative damage principle.

3.1. RAINFLOW COUNTING

The original rainflow counting formulation [12] is cumbersome to implement. The present work utilizes a later formulation [13], which is provided as part of the Wave Analysis for Fatigue and Oceanography (WAFO) Matlab toolbox for analysis of random waves and loads [14].

At each loading level, ten total stress history records were joined together to form an overall record length of $T = 16.384s$ for the rainflow cycle counting analysis. The WAFO toolbox was used to compute the turning points for each stress time history, the rainflow cycles from the sequence of turning points, and the stress ranges from the rainflow cycle count. The input stress time history data were not filtered. A histogram was computed from the stress ranges, from which the stress range PDF, $P(S_i)$, was found by

$$P(S_i) = \frac{n_i}{S_t \Delta S} \tag{5}$$

where n_i are the histogram counts, S_t is the total number of rainflow cycles, and ΔS is the PDF bin width. The number of peaks per second, $E[P]$, was determined as

$$E[P] = \frac{S_t}{T} = \frac{S_t}{16.384s}. \tag{6}$$

3.2. S-N DATA AND STRESS RATIOS

Under constant amplitude loading, the *S*-*N* curve relates the cycles to failure *N* to the applied stress range *S* via the relationship:

$$NS^m = K \tag{7}$$

where *m* and *K* are material specific properties. Typically, *S*-*N* curves are given for a range of stress ratios

$$R = S_{\min} / S_{\max} \tag{8}$$

where R is the stress ratio, and $S_{\min}$ and $S_{\max}$ are the minimum and maximum stress, respectively. For fully reversed loading, R = -1. Since this study deals with random stress histories, a statistical measure of the stress ratio is required. A simplified approach was adopted to define the minimum and maximum stress in terms its statistical moments as

$$S_{\min} = \mu - \sigma/2 \qquad S_{\max} = \mu + \sigma/2 \tag{9}$$

where μ and σ are stress mean and standard deviation, respectively.

3.3. LINEAR DAMAGE ACUMULATION

For variable amplitude loading, the Palmgren-Miner linear cumulative damage rule [15] is typically used and assumes that the damage, *D,* caused by stress cycles in one stress range can be calculated and added to damage caused by stress cycles in another stress range, or

$$D = \sum_i \frac{n_i}{N(S_i)} \tag{10}$$

where n_i is the number of cycles at stress range S_i, and $N(S_i)$ are the cycles to failure at stress range S_i. For random response, it is convenient to recast Equation (10) in the alternative form

$$D = \frac{E[P]T}{K} \sum_i S_i^m P(S_i) \Delta S \tag{11}$$

where T is the lifetime. Failure is assumed to occur when the damage sums to 1, giving the fatigue life in seconds from Equation (11) as

$$\text{Fatigue Life (s)} = \frac{K}{E[P] \sum_i S_i^m P(S_i) \Delta S} \tag{12}$$

4. RESULTS

Studies were conducted on a clamped-clamped aluminum beam measuring 18-in. × 1-in.× 0.09-in (457.2mm × 25.4mm × 2.286mm) subjected to a uniformly distributed transverse loading with a bandwidth of 1500 Hz. The following material properties were used:

$$E = 10.6 \times 10^6 \, psi \, (73.1 GPa)$$

$$G = 4.0 \times 10^6 \, psi \, (27.6 GPa)$$

$$\rho = 2.588 \times 10^{-4} \, \frac{lb_f - s^2}{in^4} \, (2768 \, \frac{kg}{m^3})$$

The MSC.NASTRAN model used for the reduced order numerical simulations consisted of 144 CBEAM elements. Simulations were run for bases B, BM, CBC and UBC. The B basis consisted of the first six symmetric bending modes. For the BM basis, the first six anti-symmetric membrane modes were added. The CBC basis consisted of the first six symmetric coupled bending-companion modes. For reasons discussed in Section 4.1, the UBC bases consisted of the first six symmetric bending and the first four dynamic companion modes. Damping was chosen to be sufficiently high so that a good comparison could be made at the peaks of the PSD. A level of mass proportional damping was specified corresponding to critical damping of 2.0% for the first symmetric bending mode.

Numerical simulation analysis in physical coordinates served as the basis for comparison of results from nonlinear modal simulation analyses. The finite element program ABAQUS was used to generate nonlinear displacement and stress time histories. The double precision explicit integration scheme with an adaptive time integration step was utilized for all analyses. The mass

proportional damping factor used was the same as that specified in the nonlinear modal simulation analyses. The ABAQUS model consisted of 144 B21 elements.

The applied loading had a Gaussian distribution and 10 ensembles of response time histories, each 2.1384*s* in duration, were simulated. The first 0.5*s* were removed from each ensemble to eliminate the transient response. Further details regarding load generation and ensemble averaging are discussed in reference [16].

Displacement results are presented at the 25% span, or 4.5-in. (114.3mm) from the clamped end. Element stresses and fatigue life estimates are presented at 0.0625-in. (1.59mm) from the clamped end (subsequently referred to as 'clamped end') and at 4.4375-in. (112.7mm) from the clamped end (subsequently referred to as 'quarter-span'). Such a choice help to elucidate the benefits and liabilities of the various modal bases under severe conditions as the ratio between membrane stress component and bending stress component is expected to vary significantly between the selected locations.

4.1. DISPLACEMENT RESPONSE

The transverse displacement PSDs are shown in Figure 5 for the lowest loading of 128 dB overall sound pressure level (OASPL). For this level, all modal bases give essentially the same results as the numerical simulation in physical DoFs. The membrane displacement PSDs for this load level, shown in Figure 6, offer a different perspective. The BM basis is the only one to compare well with the results from numerical simulation in physical DoFs. The CBC basis is inaccurate on two accounts; the magnitude is clearly incorrect and the shape of the frequency response mimics that of the bending response in Figure 5. The UBC basis accurately captures the membrane displacement frequency behavior, but the magnitudes match the physical DoFs results only between 200 and 400Hz. In the remaining bandwidth the UBC basis over-predicts

the response magnitude. Consistent with reference [17], it was found that the integration time step had to be substantially reduced compared to the other bases considered, in order to keep a stable solution for the UBC basis. For this reason, four instead of six companion modes were included in the UBC set. A static condensation in modal coordinates was proposed and demonstrated to mitigate this behavior [17], although no attempt was made to implement this scheme in the present work. Previous analysis using a four bending and four membrane mode (4+4) BM basis indicated a much better comparison with results from numerical simulation in physical DoFs, than does the above (6+4) UBC basis [18]. Further, results from the (4+4) BM basis differ only slightly from those obtained using (6+6) BM basis, in the frequency range above 1000 Hz. Therefore, the inclusion of 2 additional companion modes in the UBC basis is not expected to significantly improve the comparison with results from numerical simulation in physical DoFs. Finally, it should be noted that the BM basis, containing high frequency membrane modes, did not experience numerical integration problems. Therefore, contrary to [17], the numerical integration problem with the UBC basis does not appear to be exclusively associated with the presence of high frequency modes.

4.2. STRESS RESPONSE

The total stress PSDs at the clamped end for the excitations levels of 146, 152, and 164 dB OASPL are shown in Figure 7 to Figure 9, respectively. It is seen that the stress response at this location is dominated by the fundamental mode. As the excitation level increases, the peaks broaden and shift towards higher frequencies. The BM results compare most favorably with the solution in physical DoFs for all excitations levels studied. The responses provided by B and CBC bases are virtually the same at the excitation levels of 146 and 152 dB, and differ insignificantly at 164 dB. Bases B and CBC however exhibit some undesirable characteristics –

they do not provide the membrane contribution from the fundamental mode (no membrane peak at 120-150 Hz for the two lower loadings considered), tend to under-predict the magnitudes of higher-frequency bending-related peaks, and tend to over-predict their broadening. The UBC solution was available only for the two lower loadings considered. Results for the 164 dB loading could not be obtained because of the aforementioned stability problems. The UBC basis response captures the membrane behavior at the double frequency of the fundamental mode, but above 500 Hz the comparison between physical DoFs and UBC is the least favorable.

The quarter-span total stress PSDs for excitations of 146 and 164 dB are shown in Figure 10 and Figure 11, respectively. The stress response at this location is clearly dominated by the second bending mode. The BM basis compare most favorably with the physical DoFs solution. Bases B and CBC again result in the virtually same response at the lower excitation level, and show only minor differences at the higher excitation level. Both under-predict the bending peak magnitudes and over-predict the first membrane peak magnitude. At 146 dB, the UBC basis under-predicts the first bending and the first period-doubled peak magnitudes, and over-predicts the magnitude of second bending peak. All bases apart from BM result in an excessive third and forth peak broadening. This is most pronounced at the highest loading level.

4.3. FATIGUE ANALYSIS

The stress range PDFs for the clamped end for loadings of 146 and 164 dB are shown in Figure 12 and Figure 13, respectively. For the 146 dB level, stress range PDFs from all bases compare well with those from the physical DoFs simulation, up to approximately 6.0 ksi (41.4 MPa), above which the UBC basis is significantly lower than the rest. The highest value of stress range is reached by physical DoFs solution, followed by the B basis solution. At the 164 dB level, the stress range PDF comparison is generally worse than at 146dB, and only the BM

basis preserves a relatively good agreement with physical DoFs until approximately half of the maximum stress range, see Figure 13. Above a stress range of 42 ksi (290 MPa), the analysis in physical DoFs yields a significantly higher stress range PDF than any of the reduced order analyses. The PDF values at the high end of the stress range are most important in the fatigue estimate as these induce the most damage.

In the following fatigue life analyses, *S-N* properties for 7075-T6 aluminum [19] were used in Equation (12), as shown in Figure 14 for a range of stress ratios. In this figure, the band of maximum stress ranges corresponding to the clamped end are highlighted for the excitation levels considered. Assuming a fully reversed stress response ($R=-1$), the fatigue life ranges corresponding to the upper and lower 90% confidence intervals of the stress are shown in Table 1. These fatigue estimates were obtained by scaling the stress time histories such that their RMS values corresponded to the upper and lower bounds of the 90% confidence interval. At the 146 dB excitation level, the shortest fatigue life is estimated using the lower bound of the 90% confidence interval for the physical DoFs solution. The longest fatigue life is estimated by the upper bound of the 90% confidence interval for the UBC basis. These are consistent with the stress range PDFs shown in Figure 12. For the 164 dB excitation, the estimated fatigue life ranges corresponding to physical DoFs and B basis solutions are the shortest and are almost identical, consistent with the close agreement of their stress range PDFs shown in Figure 13. Estimates computed from both the BM and CBC bases indicate a longer (non-conservative) life. Estimates computed using the UBC basis are the most non-conservative through the range of loadings considered.

Note that maximum stress ranges at the 146 and 152 dB levels fall at or below the fatigue life run-out. In this region, small differences in stress range cause large changes in the fatigue life estimate. For this reason, fatigue life estimates for all but the UBC basis are considered quite good at the 146 and 152 dB levels, even if they are non-conservative. Also note that while the maximum stress range exceeded the material yield stress of 72 ksi (496 MPa) for the 164 dB loading, the maximum stress itself was less than 50 ksi (345 MPa). Therefore, material nonlinearity was not introduced.

Although the fatigue life of this particular beam structure under investigation will be dictated by the damage accumulated at the clamped end, it is of interest to investigate the quality of fatigue life estimates at the quarter-span location, where the effect of membrane stress is more significant. Stress range PDFs for the quarter-span location are shown in Figure 15 and Figure 16 for the 146 dB and 164 dB loading levels, respectively. Corresponding fatigue life estimates are given in Table 1. For the 146 dB excitation level, all stress ranges compare well up to 2 ksi (13.8 MPa). Beyond this stress range, the physical DoFs and UBC basis have higher stress range PDFs than the B, BM, and CBC solutions. The fatigue life estimated by physical DoFs and UBC is the shortest, and compare very well with each other. Estimates made using the B, BM, and CBC bases, are comparable to each other, but overestimate the fatigue life approximately by a factor of 2. Since S-N data for the 146 dB and 152 dB level is well beyond run-out, small differences in the stress range PDF result in large difference in the fatigue life estimate. From a practical perspective, the difference between any of the bases and physical DoFs is insignificant. The advantage of using the BM basis becomes apparent as the response becomes more nonlinear with increasing excitation load. For the 164 dB level, the stress range PDFs of physical DoFs and BM solutions, shown in Figure 16, compare very well, as do their fatigue estimates. Life

estimates obtained with B basis are shortest, indicating a conservative fatigue estimate. At the quarter-span location, the membrane to bending stress ratio is higher than at the clamped end of the beam. It is therefore expected that the BM basis produces an accurate fatigue estimate at 164 dB, where nonlinear effects are the most significant. Although the CBC basis also produces an accurate fatigue life estimate at 164 dB, its performance is inconsistent, since at the excitation level of 152 dB the CBC estimate is the worst.

4.4. EFFECT OF MEAN STRESS

To gain additional insight into how the differences in the predicted stress response are reflected in the fatigue calculation, the mean μ and standard deviation σ of the total stress are shown in Table 2 and Table 3, respectively. The BM basis is the only one to accurately capture the mean value predicted by simulation in physical DoFs for both clamped and quarter-span locations. The B and CBC bases both result in nearly zero mean stress for the clamped end and over-predict mean stress at the quarter-span location. The UBC basis shows the opposite trend of over-predicting the mean value at the clamped end and under-predicting it at the quarter-span. In all the cases considered in this study, results computed using the reduced order simulation underestimated the standard deviation obtained from simulation in physical DoFs, as shown in Table 3. Overall, the best comparisons with physical DoFs solutions were obtained using the BM basis. As in the case of mean stress, the B and CBC bases again resulted in very similar total stress standard deviations. Inaccuracies in stress mean and standard deviation can affect the fatigue life estimation in two ways. First, the differences alter the calculated stress range PDF and consequently the fatigue life. Further, these differences alter the stress ratio *R*, which dictates the particular *S-N* data used.

With regard to the effect on stress range PDF, it is helpful to investigate the rainflow counting (RFC) matrix. The RFC matrix for the clamped end at the 152 dB loading is shown in Figure 17 and Figure 18. The BM basis, which correctly predicts the total stress mean, is similarly skewed as the physical DoFs solution, as shown in Figure 17. The skewness (λ) of the total stress for the BM basis is 0.26 versus 0.30 for the analysis in physical DoFs. Recall from Figure 2, that the membrane stress component alone accounts for the mean value and hence for the skewness of the total stress response. By contrast, the B and CBC bases, which have near zero mean stress, are not skewed and form min-max stress counts along the dashed line of Figure 17 and Figure 18. The UBC basis overestimates the total stress mean and results in a slightly excessive skewness of 0.33. Finally, the maximum stress indicated by the solution in physical DoFs exceeds all of the reduced order analyses, in agreement with the standard deviation of Table 3.

From the data presented in Table 2, it is seen that the mean stress increases as the excitation level increases, due to increasing nonlinear response. This alters the stress ratio as per Equations (8) and (9), dictating the use of a different S-N curve from the data in Figure 14. To demonstrate the effect of stress ratio, the fatigue life at the clamped end for the 152 dB loading was re-evaluated. Stress ratios were calculated using the total stress mean and the standard deviations from Table 2 and Table 3, respectively. For the physical DoFs solution, and BM and UBC bases, the computed stress ratio and corresponding fatigue life estimates are shown in Table 4. In all cases, fatigue life estimates shown were obtained directly from the stress time history, not the 90% confidence intervals, as shown in Table 1. The effect of using the actual stress ratio shifts the *S-N* curve to the right and results in a longer fatigue life estimate. Since the B and CBC bases produced nearly zero total stress mean values, the stress ratio calculated through this procedure would inaccurately indicate a fully reversed value of $R = -1$. Figure 19 and Figure 20

show the reason why the total stress mean obtained using the B and CBC bases for this case is deficient. The bending stress in Figure 19 indicates the same mean value for all analyses. However, relative to the physical DoFs analysis results, the B and CBC bases grossly underestimate the membrane stress component throughout the entire frequency range, as shown in Figure 20. The most significant effect on the membrane mean stress comes from its zero frequency component, which is reduced by more than 2 orders of magnitude when compared to the physical DoFs analysis mean value.

An alternative approach to computing the stress ratio for B and CBC analysis was undertaken, following the approach proposed in reference [20]. For a range of applied random loading, the RMS transverse deflection at the mid-span of the beam was found. A static analysis was then performed with the same load distribution such that it produced the same static deflection at the mid-span as the RMS deflection. For the particular location of interest, the ratio between static membrane and bending stress was found. Using the assumption that the ratio of RMS membrane to bending stress was the same as static membrane to bending stress, the RMS membrane stress can be estimated from

$$\left(S_{\text{membrane}}\right)_{\text{RMS}} \approx \left(S_{\text{bending}}\right)_{\text{RMS}} \left(S_{\text{membrane}} / S_{\text{bending}}\right)_{\text{Static}} \tag{13}$$

where $(S_{bending})_{RMS}$ is obtained from the time history of the bending stress. Further assuming that the membrane response is dominated by a single mode, the membrane mean can be written as

$$\left(S_{\text{membrane}}\right)_{\text{Mean}} = \tfrac{1}{2}\left(S_{\text{membrane}}\right)_{\text{Peak}} = \tfrac{\sqrt{2}}{2}\left(S_{\text{membrane}}\right)_{\text{RMS}} \quad . \tag{14}$$

Finally, since the mean value of the total stress is due solely to membrane stretching, the mean value of the total stress and the standard deviation can be expressed as

$$\mu = \left(S_{\text{membrane}}\right)_{\text{Mean}}, \qquad \sigma = \tfrac{1}{2}\left(S_{\text{bending}}\right)_{\text{RMS}} \quad . \tag{15}$$

For the case considered, the presented total stress mean static correction yielded fairly accurate stress ratios, as denoted in Table 4. All reduced modal fatigue estimates remained non-conservative relative to the results obtained from the physical DoFs analysis.

4.5. FATIGUE SENSITIVITY TO TOTAL STRESS MAGNITUDE AND FREQUENCY

An analysis of the total stress PSD plots reveals three manners in which the various analyses differ from each other, i.e. differences in stress magnitude, frequency shift in the nonlinear regime, and peak broadening. The latter factor is very difficult to quantify in a nonlinear regime, however sensitivity studies of the first two factors can be conducted with reasonable accuracy. Certainly, all of the above properties are related, but knowledge of which one of them is more likely to have a larger impact on the predicted fatigue life can help target future improvements to the analysis.

Results from the physical DoFs analysis were selected as a basis for the sensitivity studies. For both studies, the total stress time histories were operated on and fatigue life predictions were made using the method described in Section 3. The fatigue life sensitivity to stress magnitude was determined by simply scaling the time history. The sensitivity to frequency was determined by scaling the timebase. In each case, a scaling of 1, 5 and 10 percent was applied, as such differences spanned the range of those observed between the various modal bases and the solution in physical DoFs.

Figure 21 shows the effect of stress magnitude and frequency scaling, expressed as a percentage of fatigue life relative to the original data. For the range of scaling considered, the fatigue life is shown to be more sensitive to the stress magnitude than to frequency. The sensitivity to frequency shift is shown to vary linearly, as suggested by Equation (10). The sensitivity to stress magnitude varies nonlinearly, reflecting the nonlinear character of the S-N

data. Not shown is that these relationships are identical irrespective of the original load level chosen.

5. CONCLUSIONS

The effect of modal basis selection on displacement response, stress response and fatigue life estimation using a nonlinear modal simulation was investigated. With regard to displacement and stress response, for the case considered, it was found that

- the bending and membrane modal basis offered the only accurate prediction of membrane displacement and the best prediction of bending, membrane and total stress,
- the bending modes only basis offered the second best approach as it did not produce anomalous behavior in the displacement PSDs, did not increase the size of the coupled set of modal equations, allowed for the largest integration time step of all bases, and did not have the added complication of identifying membrane modes or computing companion modes,
- the CBC basis produced non-physical behavior in the membrane displacement PSDs, and therefore its use is not recommended,
- inclusion of mass normalized UBC modes required significantly smaller integration time steps than for any other bases considered.

With regard to fatigue life estimates, at the clamped end, it was found for the case considered that

- all modal bases variants gave non-conservative estimates of fatigue life relative to that obtained through simulation in physical DOFs, and

- fatigue life estimates from the B, BM and CBC bases were comparable to each other, and estimates made using the UBC basis significantly differed.

It was further found that

- accurate membrane stress modeling is important at all locations; the static membrane stress affects the stress ratio and consequently the selection of S-N curve used for fatigue estimation,
- the B and CBC bases were incapable of accurate membrane stress modeling at certain locations and consequently yielded inaccurate stress ratios; a procedure was developed to estimate the static mean stress for such cases,
- for the case considered when $R \neq -1$, all reduced order modal fatigue estimates at the clamped end remained non-conservative relative to the results obtained from the physical DoFs analysis, and
- fatigue life estimates were more sensitive to changes in the stress magnitude, than to changes in the peak frequencies.

Finally, at the quarter span, it was found that the modal bases sometimes gave conservative estimates and sometimes gave non-conservative estimates of fatigue life. Due to the higher contribution of membrane to bending stress at this location, the BM basis provides the most accurate fatigue life estimate due to its better ability to model the membrane component.

REFERENCES

[1] Mei, C., Dhainaut, J.M., Duan, B., Spottswood, S.M., and Wolfe, H.F., "Nonlinear random response of composite panels in an elevated thermal environment," Air Force Research Laboratory, Wright-Patterson Air Force Base, OH, AFRL-VA-WP-TR-2000-3049, October 2000.

[2] Przekop, A., "Nonlinear response and fatigue estimation of aerospace curved surface panels to combined acoustic and thermal loads," *Ph.D. Dissertation*, Old Dominion University, 2003.

[3] Przekop, A., Guo, X., Azzouz, M.S., and Mei, C., "Reinvestigation of nonlinear random response of shallow shells using finite element modal formulation," *Proceedings of the 45th AIAA/ASME/ASCE/AHS/ASC Structures, Structural Dynamics and Materials Conference*, AIAA-2004-1553, Palm Springs, CA, 2004.

[4] McEwan, M.I., Wright, J.R., Cooper, J.E., and Leung, Y.T., "A finite element/modal technique for nonlinear plate and stiffened panel response prediction," *Proceedings of the 42nd AIAA/ASME/ASCE/AHS/ASC Structures, Structural Dynamics, and Materials Conference*, AIAA-2001-1595, Seattle, WA, 2001.

[5] Muravyov, A.A. and Rizzi, S.A., "Determination of nonlinear stiffness with application to random vibration of geometrically nonlinear structures," *Computers and Structures*, Vol. 81, No. 15, pp. 1513-1523, 2003.

[6] Rizzi, S.A. and Przekop, A., "The effect of basis selection on thermal-acoustic random response prediction using nonlinear modal simulation," *Proceedings of the 45th AIAA/ASME/ASCE/AHS/ASC Structures, Structural Dynamics and Materials Conference*, AIAA-2004-1554, Palm Springs, CA, 2004.

[7] Hollkamp, J.J., Gordon, R.W., and Spottswood, S.M., "Nonlinear sonic fatigue response prediction from finite element modal models: a comparison with experiments," *Proceedings of the 44th AIAA/ASME/ASCE/AHS/ASC Structures, Structural Dynamics, and Materials Conference*, AIAA-2003-1709, Norfolk, VA, 2003.

[8] Mignolet, M.P., Radu, A.G., and Gao, X., "Validation of reduced order modeling for the prediction of the response and fatigue life of panels subjected to thermo-acoustic effects," *Structural Dynamics: Recent Advances, Proceedings of the 8th International Conference*, Southampton, UK, 2003.

[9] Press, W.H., Teukolsky, S.A., Vetterling, W.T., and Flannery, B.P., "Numerical recipes, the art of scientific computing," CDROM v2.10, Cambridge University Press, 2002.

[10] Rizzi, S.A. and Muravyov, A.A., "Improved equivalent linearization implementations using nonlinear stiffness evaluation," NASA TM-2001-210838, March 2001.

[11] Dowling, N.E., "Fatigue failure predictions for complicated strain-stress histories," *Journal of Materials*, Vol. 7, pp. 71-87, 1972.

[12] Matsuishi, M. and Endo, T., "Fatigue of metals subjected to varying stress," *Japan Society of Mechanical Engineers*, Fukuoka, Japan, March, 1968.

[13] Rychlik, I., "A new definition of the rainflow cycle counting method," *International Journal of Fatigue*, Vol. 9, No. 2, pp. 119-121, 1987.

[14] "WAFO - A Matlab toolbox for analysis of random waves and loads," Version 2.0.02, The WAFO Group, Lund Institute of Technology, Lund University, 2000.

[15] Miner, M.A., "Cumulative damage in fatigue," *Trans. ASME, Journal of Applied Mechanics*, Vol. 67, pp. A159-A164, 1945.

[16] Rizzi, S.A. and Muravyov, A.A., "Comparison of nonlinear random response using equivalent linearization and numerical simulation," *Structural Dynamics: Recent Advances, Proceedings of the 7th International Conference*, Vol. 2, pp. 833-846, Southampton, UK, 2000.

[17] Radu, A.G., Yang, B., Kim, K., and Mignolet, M.P., "Prediction of the dynamic response and fatigue life of panels subjected to thermo-acoustic loading," *Proceedings of the 45th AIAA/ASME/ASCE/AHS/ASC Structures, Structural Dynamics and Materials Conference*, AIAA-2004-1557, Palm Springs, CA, 2004.

[18] Przekop, A. and Rizzi, S.A., "Reduced order methods for prediction of thermal-accoustic fatigue," *Proceedings of The Seventh International Conference on Computational Structures Technology, B.H.V. Topping and C.A. Mota Soares, (Editors), Civil-Comp Press, Stirling, United Kingdom, paper 84, September 2004.*, Lisbon, Portugal, 2004.

[19] "Military handbook MIL-HDBK-5H: Metallic materials and elements for aerospace vehicle structures," Knovel Interactive Edition, 2003.

[20] Rizzi, S.A., "On the use of equivalent linearization for high-cycle fatigue analysis of geometrically nonlinear structures," *Structural Dynamics: Recent Advances, Proceedings of the 8th International Conference*, Southampton, UK, 2003.

FIGURE CAPTIONS

Figure 1: Quarter-span total stress time history at different load levels.

Figure 2: Quarter-span component stress probability density at 164 dB.

Figure 3: Quarter-span component stress PSD at 128 dB.

Figure 4: Quarter-span component stress PSD at 164 dB.

Figure 5: Quarter-span transverse displacement PSD at 128 dB.

Figure 6: Quarter-span membrane displacement PSD at 128 dB.

Figure 7: Total stress PSD at clamped end for 146 dB loading.

Figure 8: Total stress PSD at clamped end for 152 dB loading.

Figure 9: Total stress PSD at clamped end for 164 dB loading.

Figure 10: Total stress PSD at quarter-span for 146 dB loading.

Figure 11: Total stress PSD at quarter-span for 164 dB loading.

Figure 12: Stress range PDF at clamped end for 146 dB loading.

Figure 13: Stress range PDF at clamped end for 164 dB loading.

Figure 14: *S*-*N* curves for different stress ratios [19].

Figure 15: Stress range PDF at quarter-span for 146 dB loading.

Figure 16: Stress range PDF at quarter-span for 164 dB loading.

Figure 17: Total stress RFC matrix at clamped end for 152 dB loading for B and BM bases.

Figure 18: Total stress RFC matrix at clamped end for 152 dB loading for companion bases.

Figure 19: Clamped end bending stress for 152 dB loading.

Figure 20: Clamped end membrane stress for 152 dB loading.

Figure 21: Sensitivity of fatigue life to changes in stress magnitude and frequency.

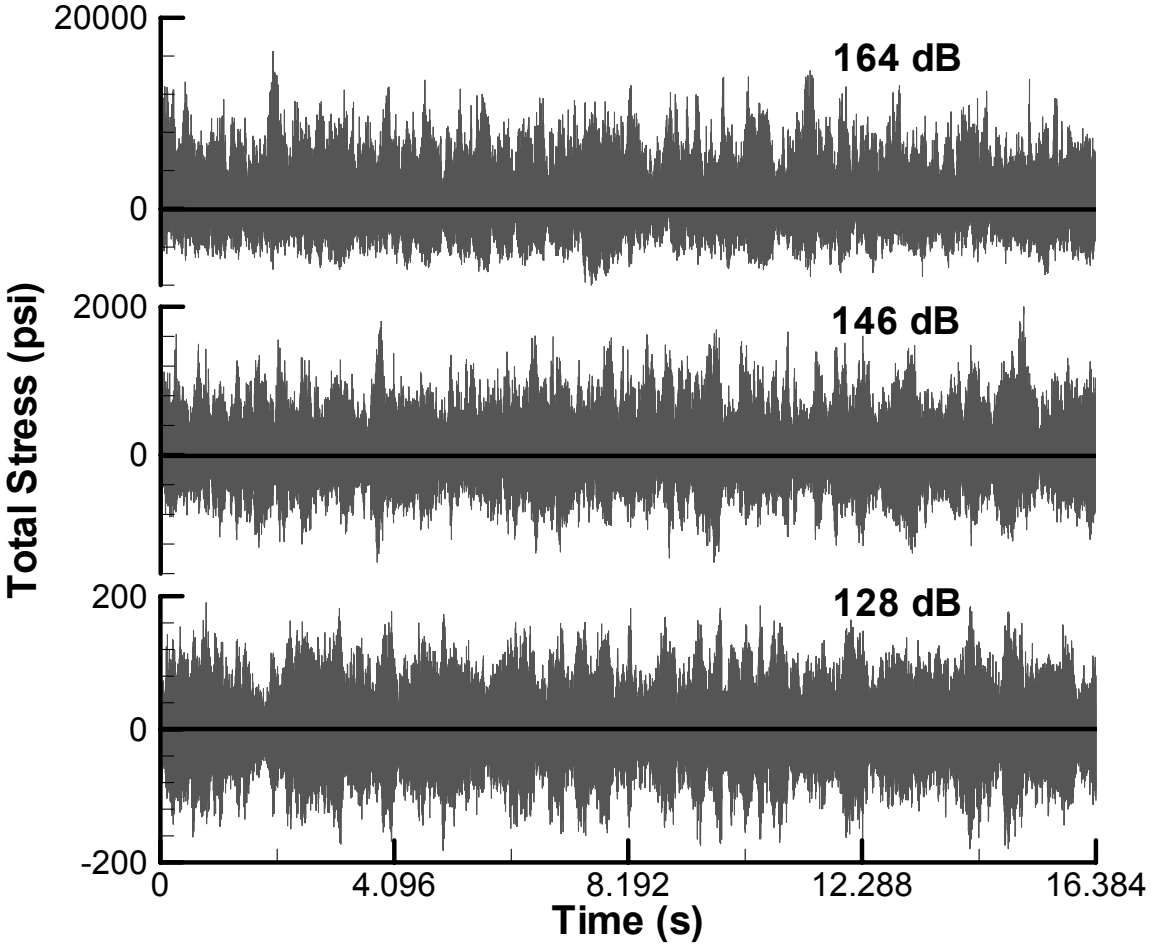

Figure 1: Quarter-span total stress time history at different load levels.

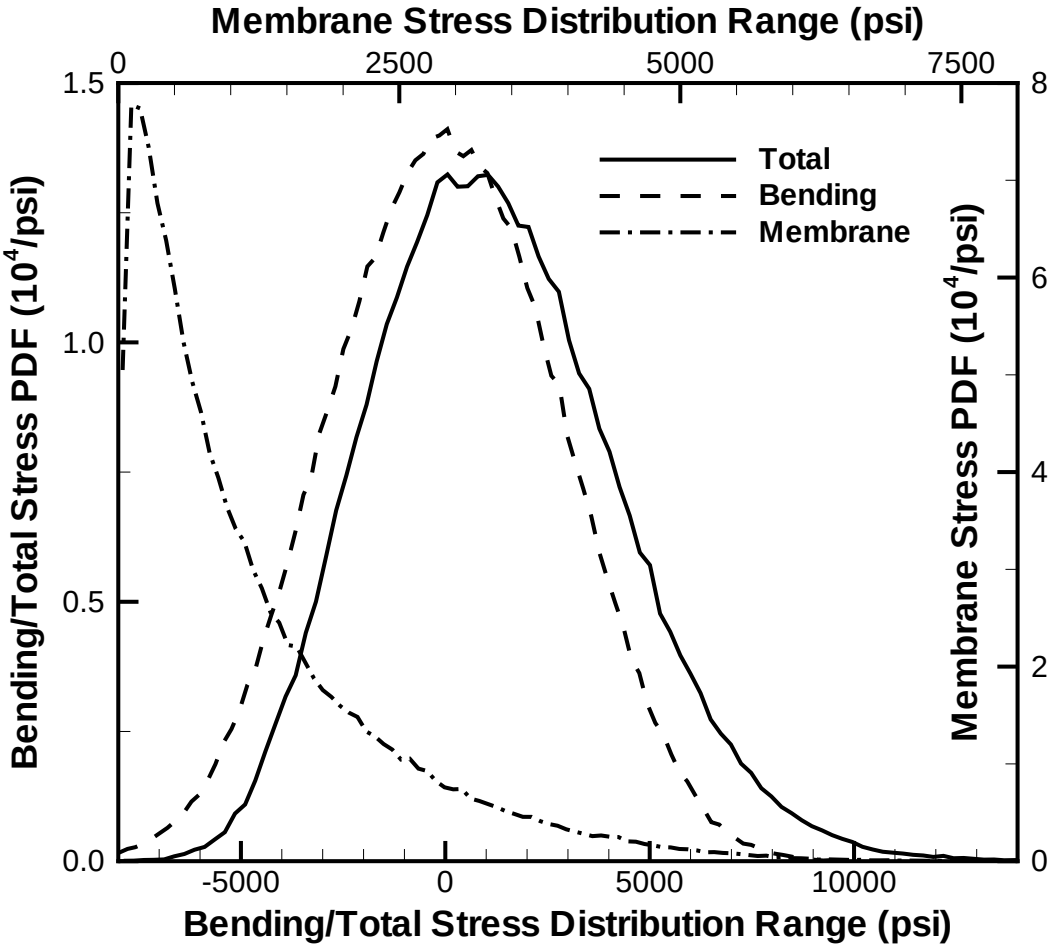

Figure 2: Quarter-span component stress probability density at 164 dB.

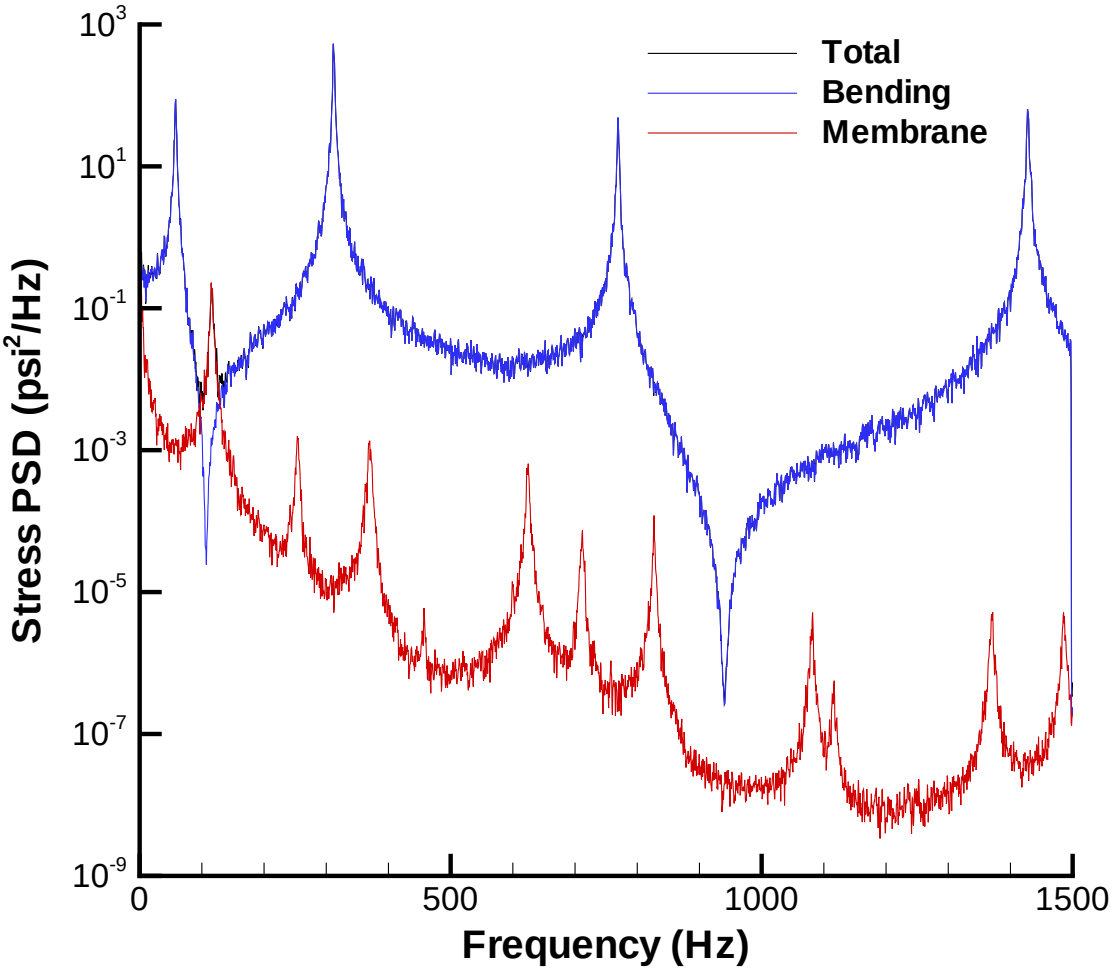

Figure 3: Quarter-span component stress PSD at 128 dB.

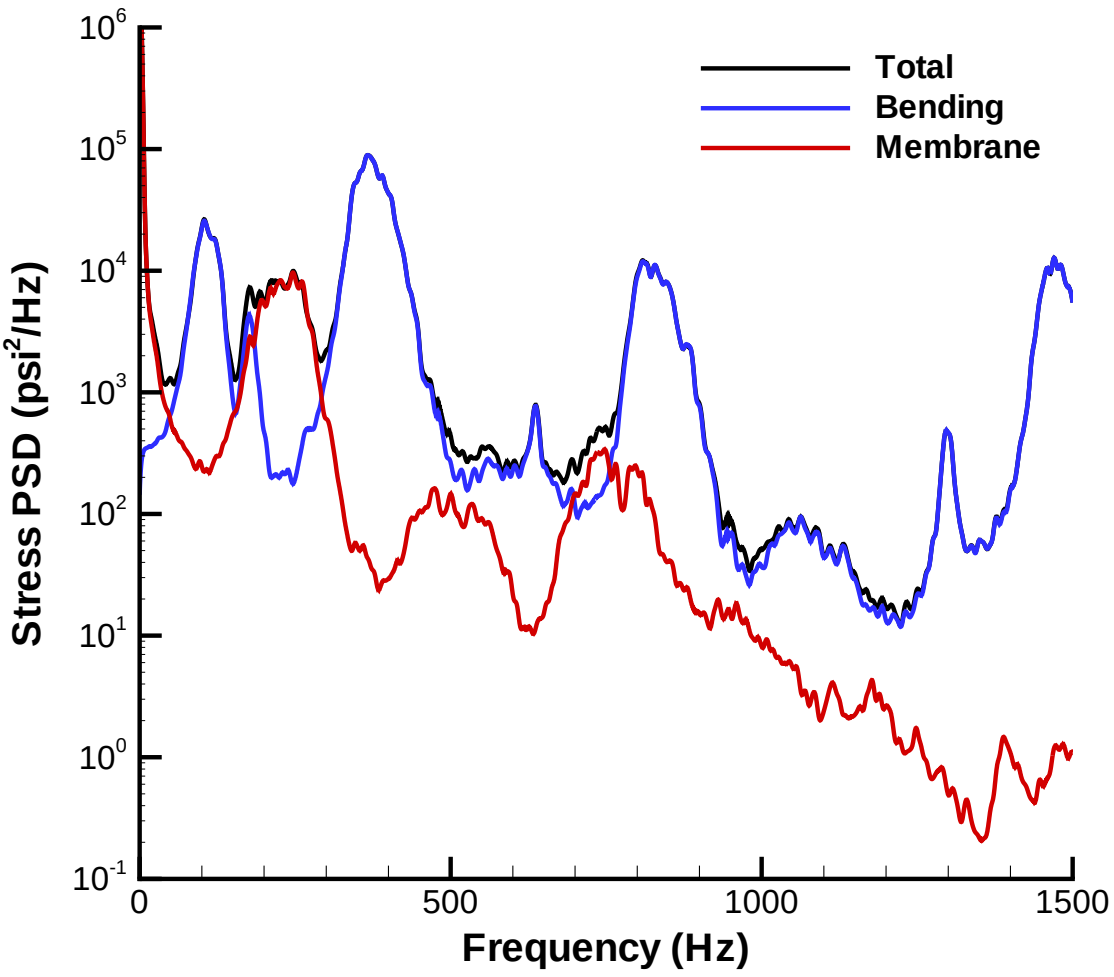

Figure 4: Quarter-span component stress PSD at 164 dB.

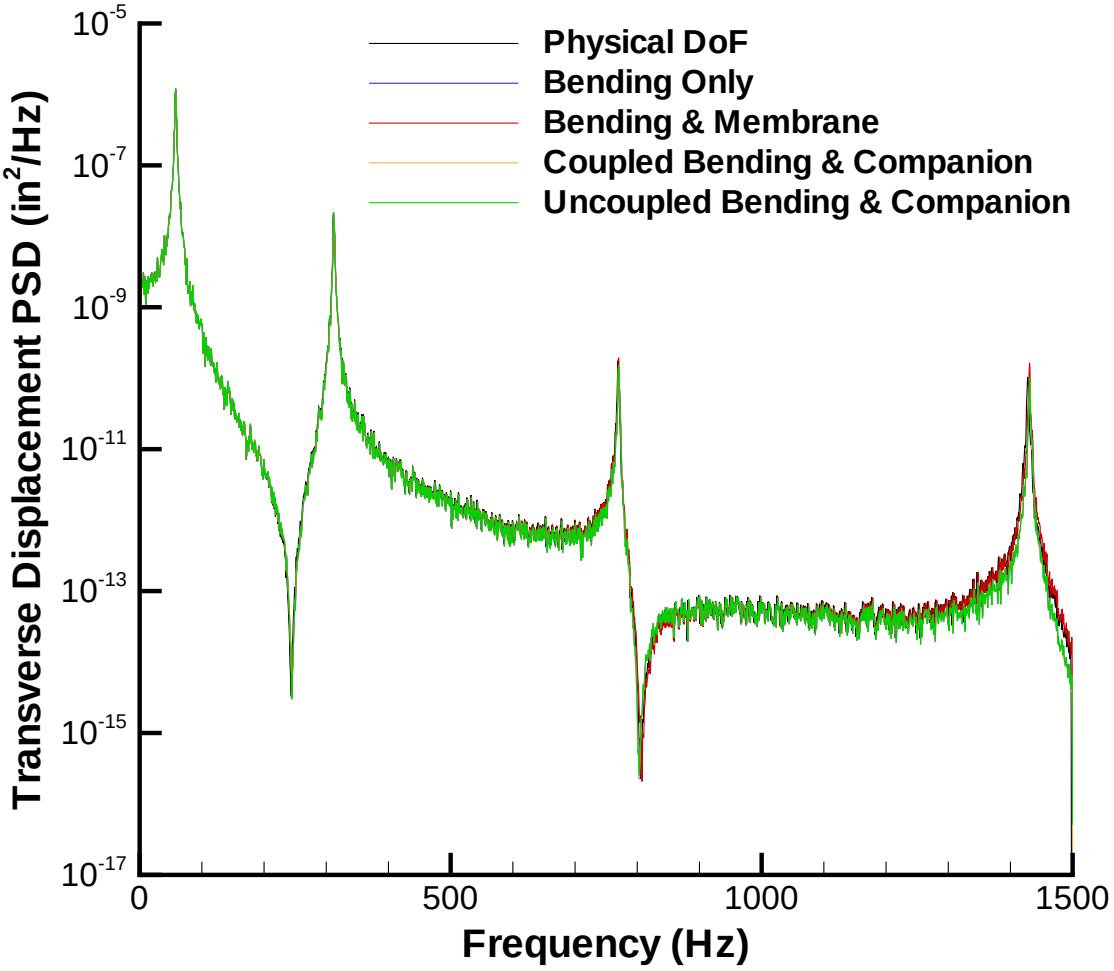

Figure 5: Quarter-span transverse displacement PSD at 128 dB.

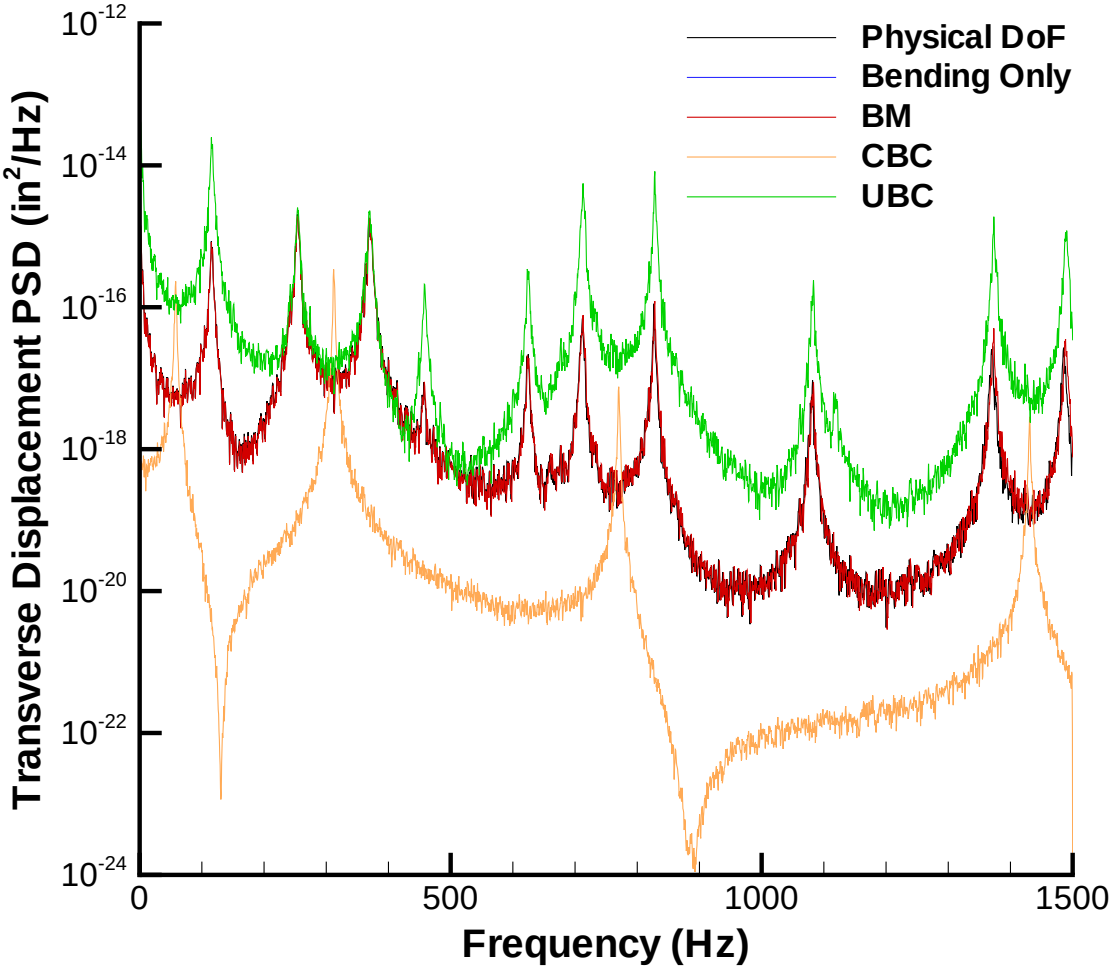

Figure 6: Quarter-span membrane displacement PSD at 128 dB.

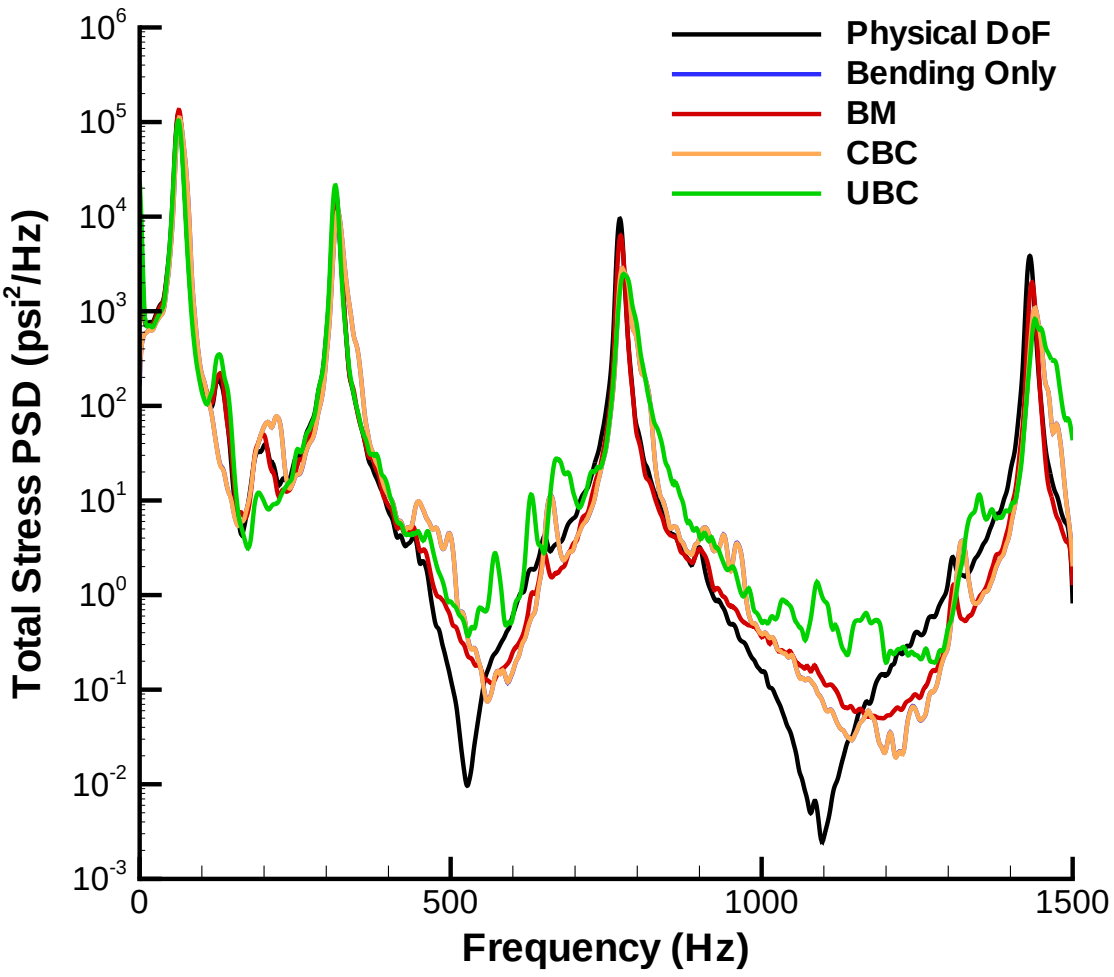

Figure 7: Total stress PSD at clamped end for 146 dB loading.

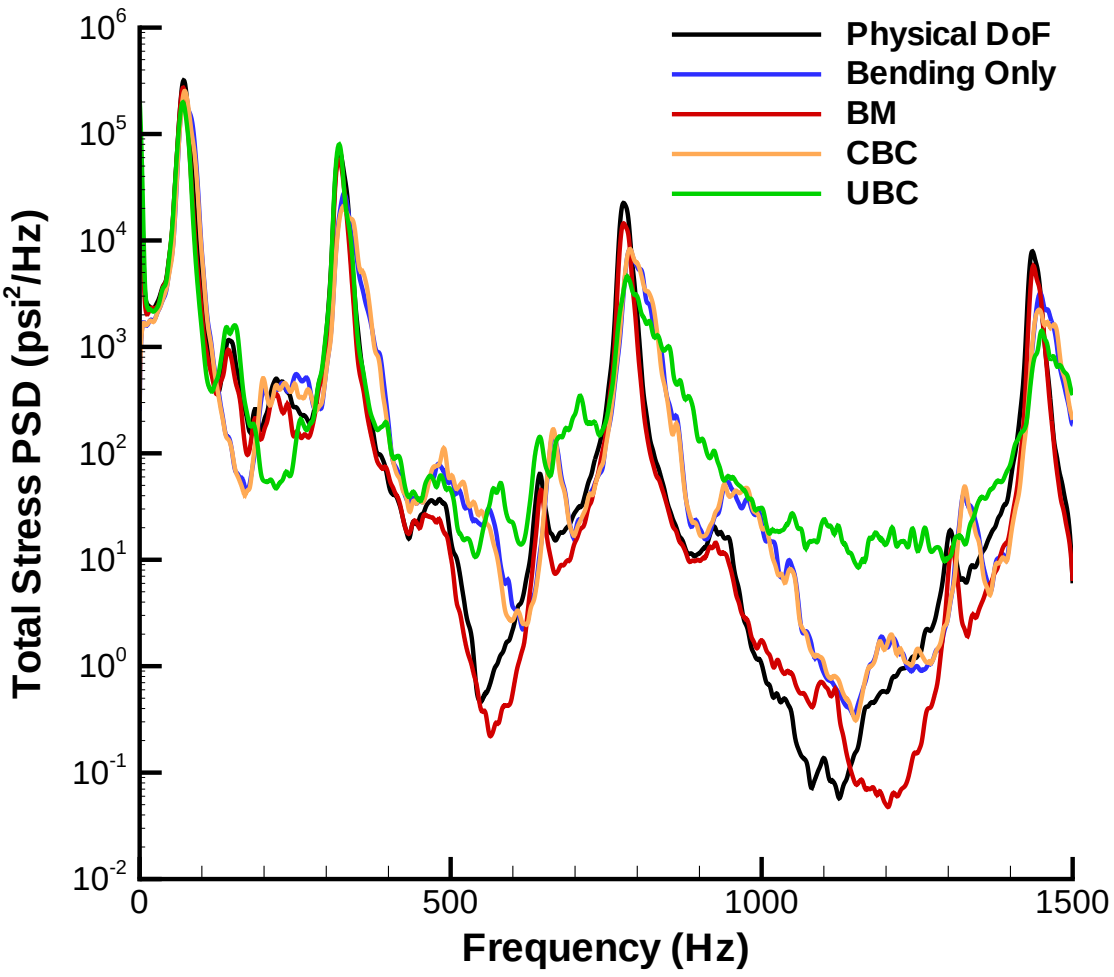

Figure 8: Total stress PSD at clamped end for 152 dB loading.

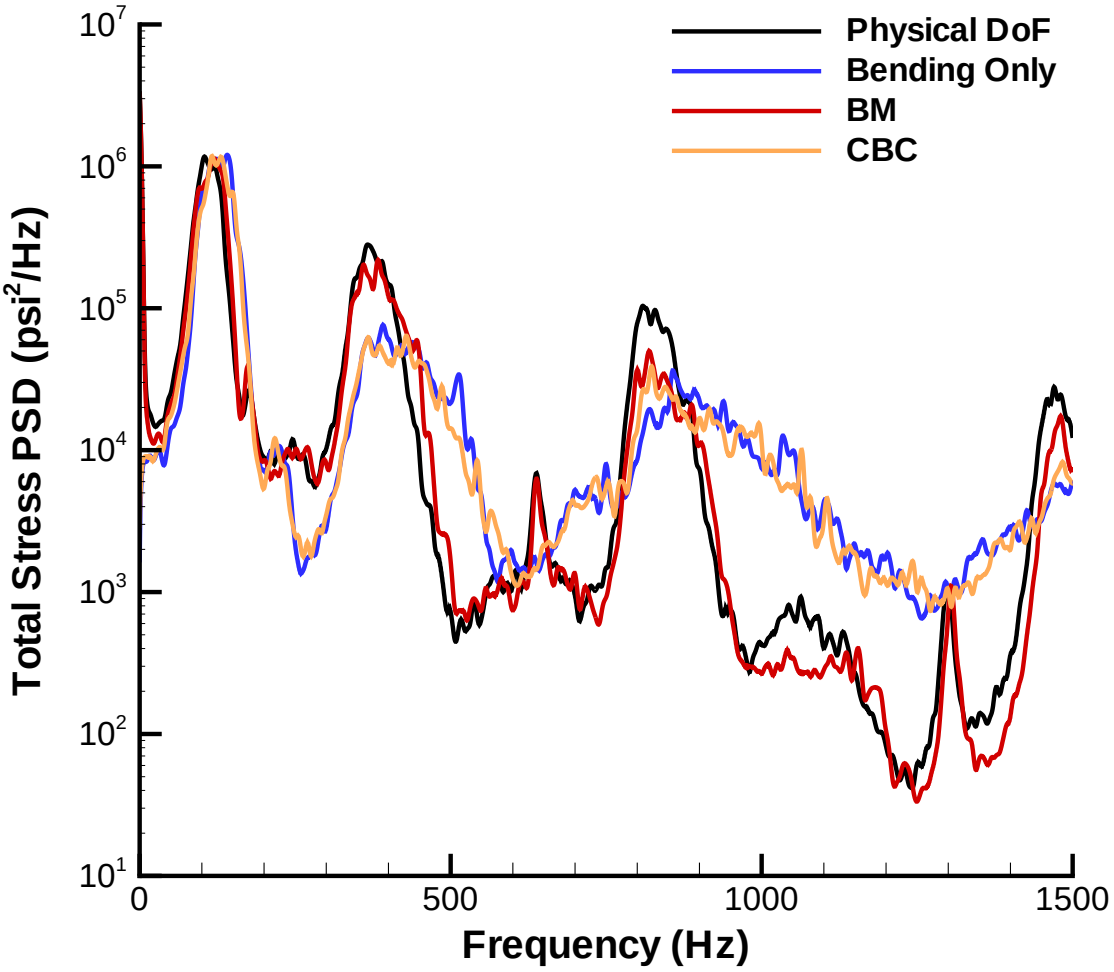

Figure 9: Total stress PSD at clamped end for 164 dB loading.

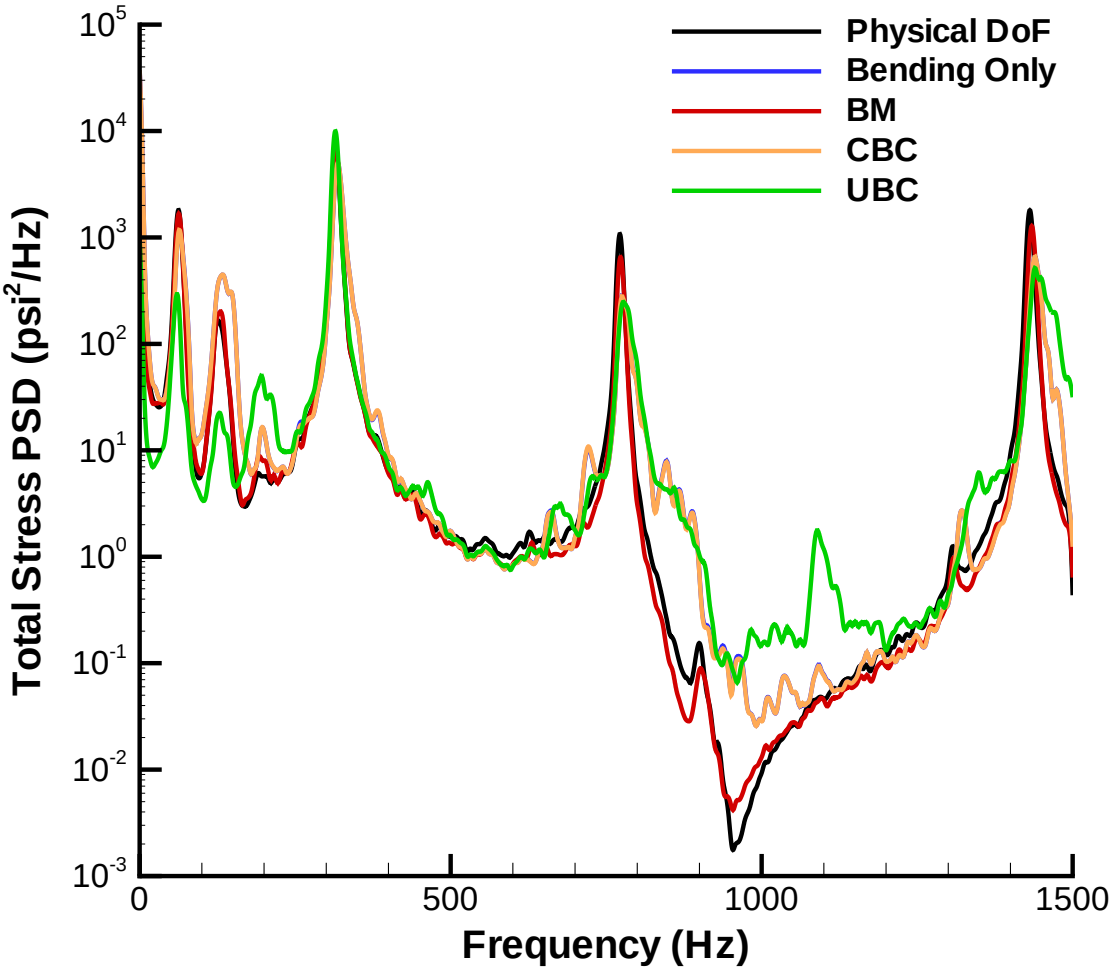

Figure 10: Total stress PSD at quarter-span for 146 dB loading.

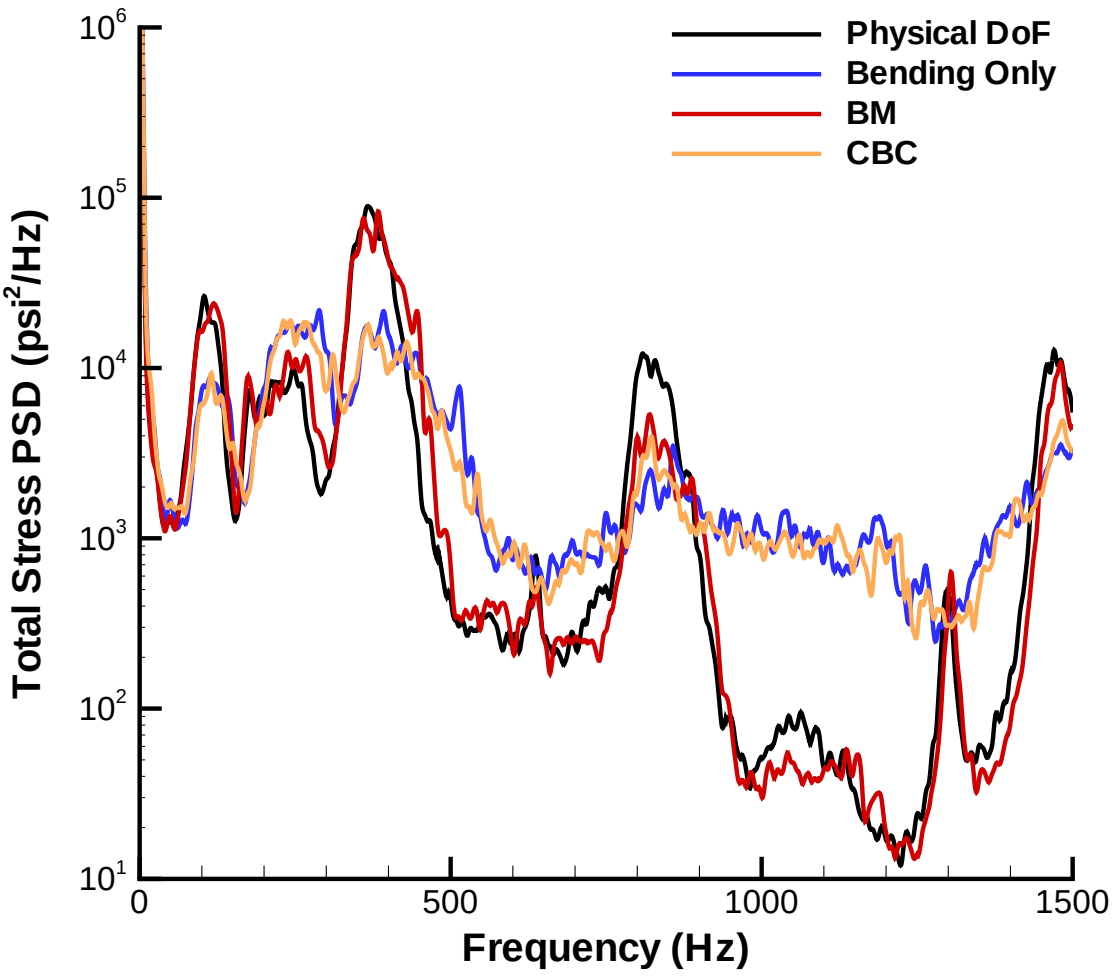

Figure 11: Total stress PSD at quarter-span for 164 dB loading.

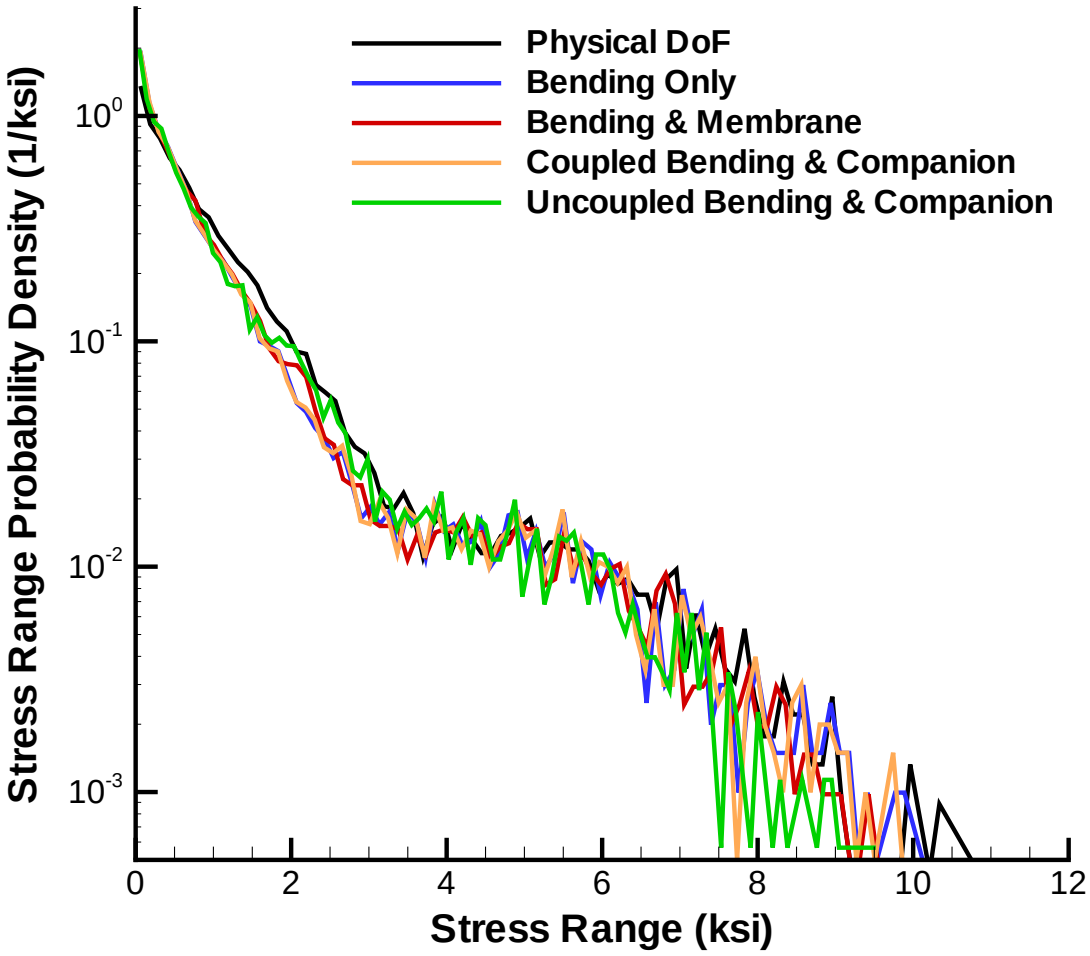

Figure 12: Stress range PDF at clamped end for 146 dB loading.

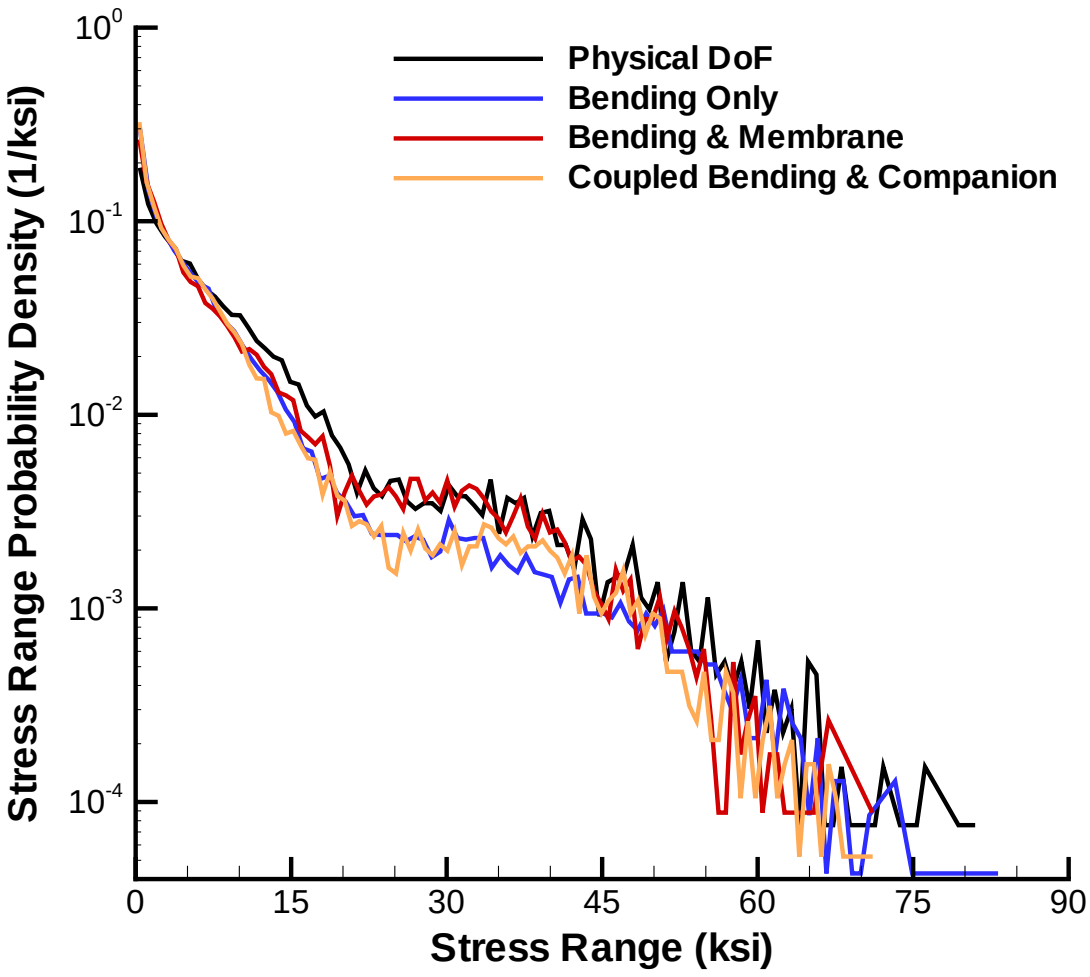

Figure 13: Stress range PDF at clamped end for 164 dB loading.

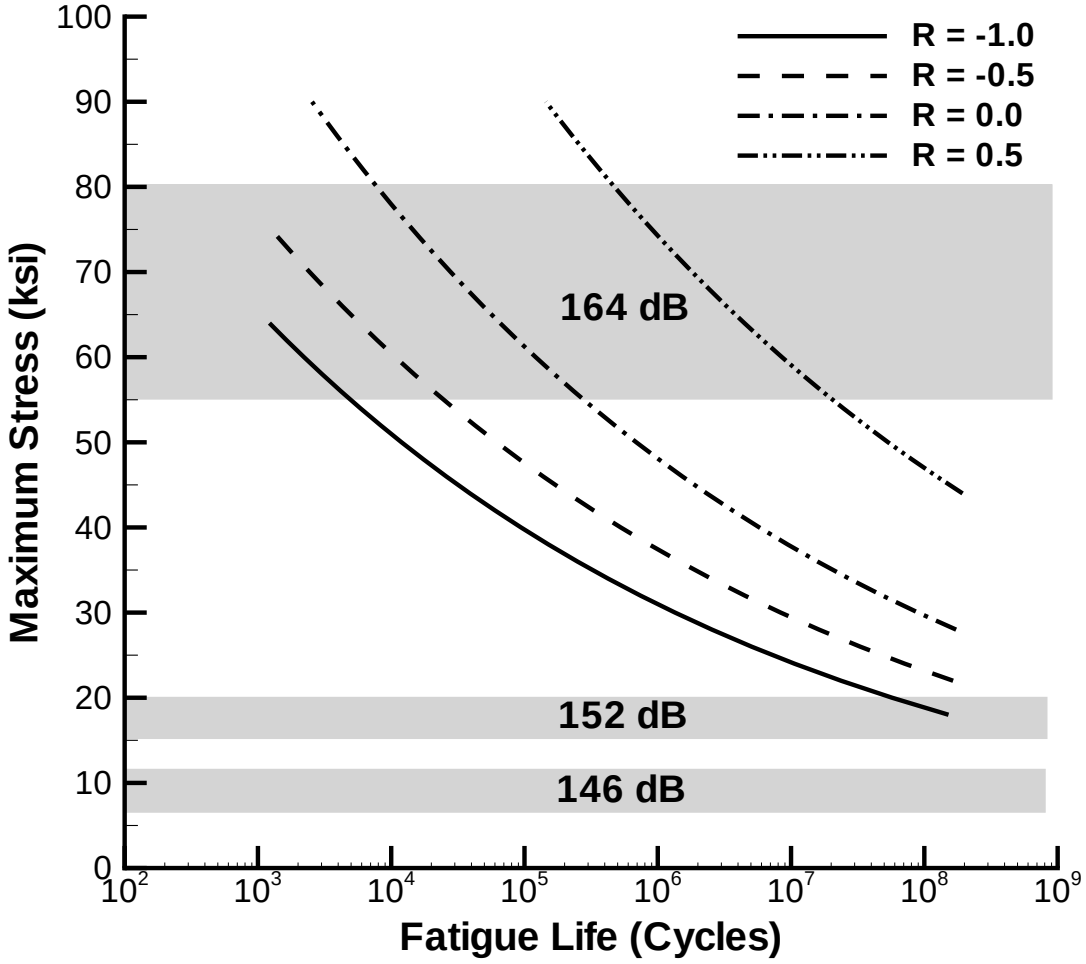

Figure 14: *S-N* curves for different stress ratios [19].

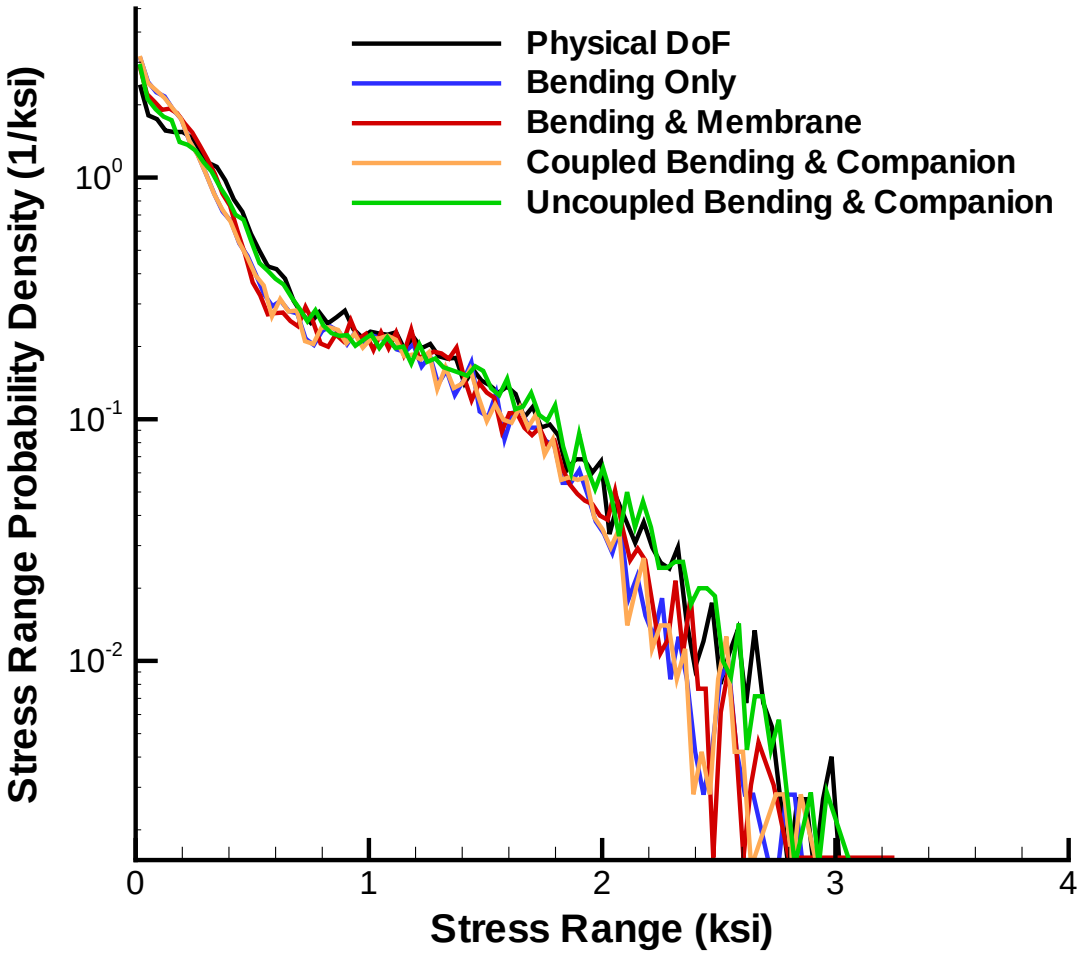

Figure 15: Stress range PDF at quarter-span for 146 dB loading.

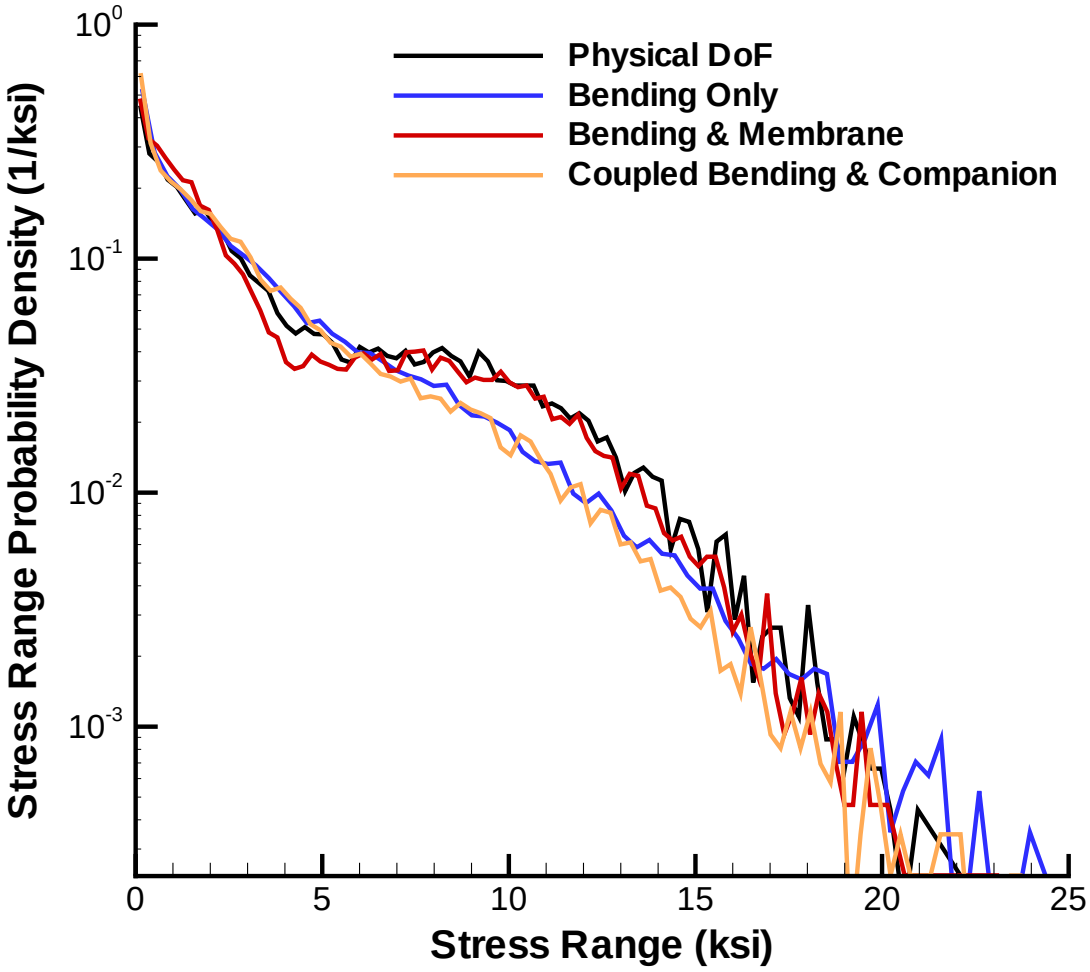

Figure 16: Stress range PDF at quarter-span for 164 dB loading.

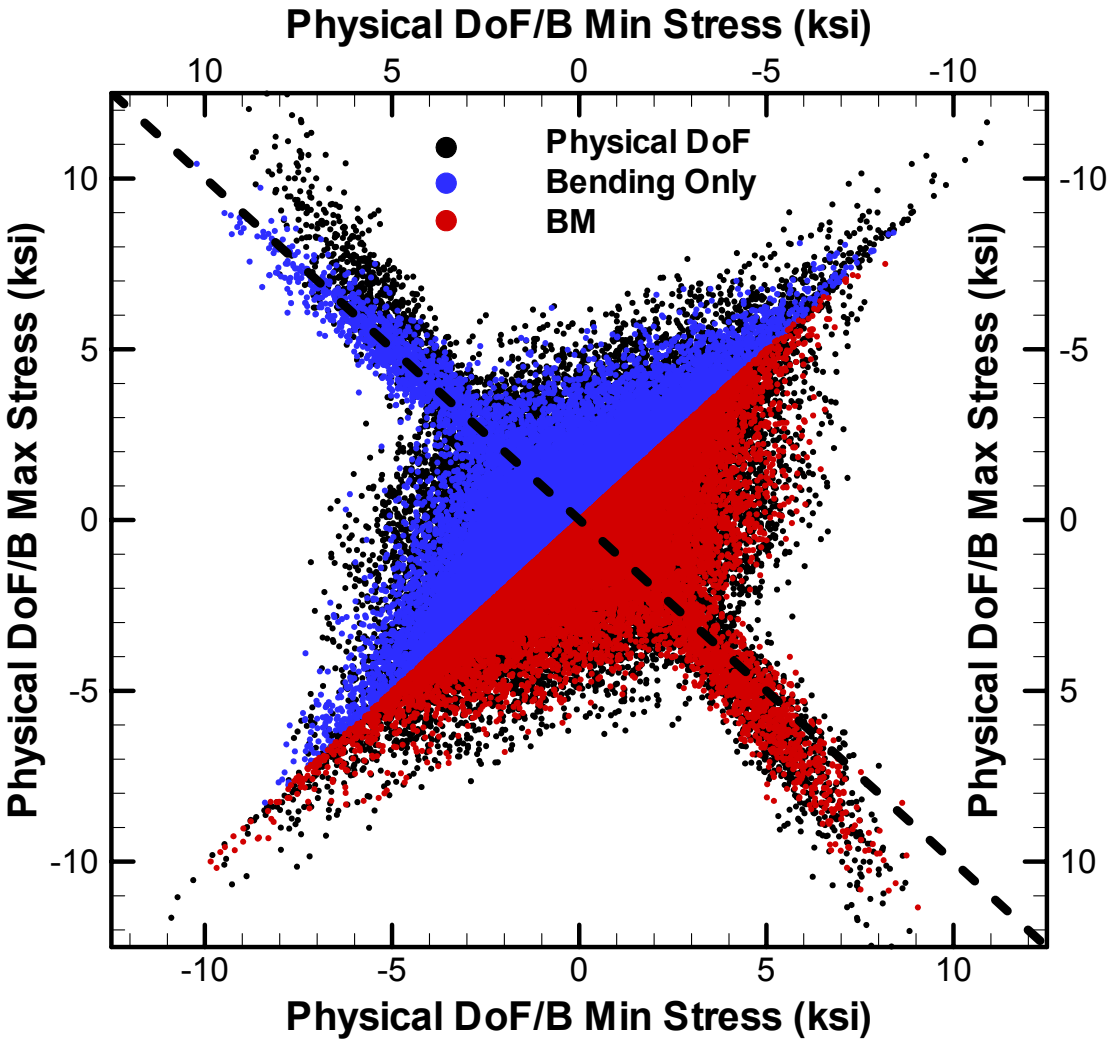

Figure 17: Total stress RFC matrix at clamped end for 152 dB loading for B and BM bases.

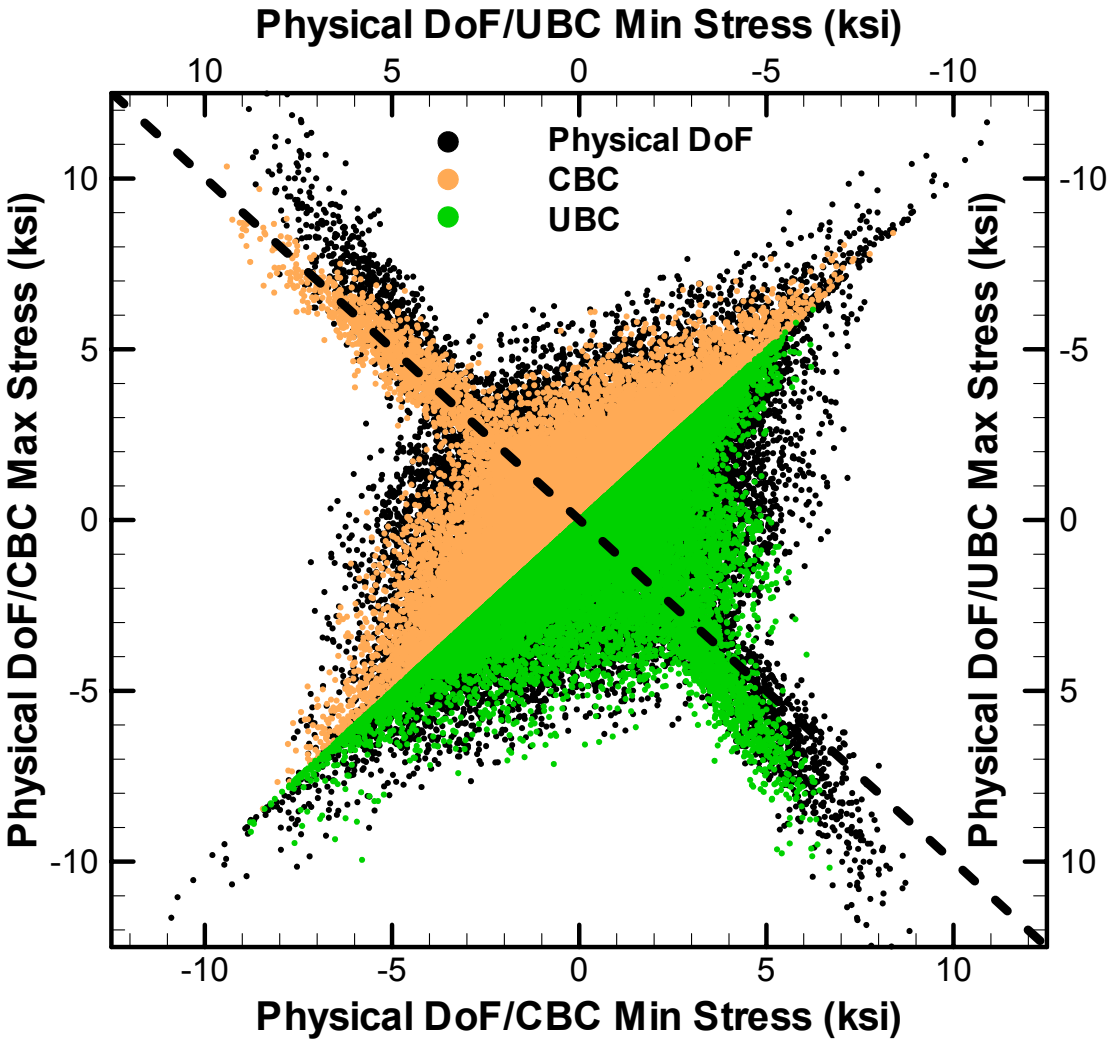

Figure 18: Total stress RFC matrix at clamped end for 152 dB loading for companion bases.

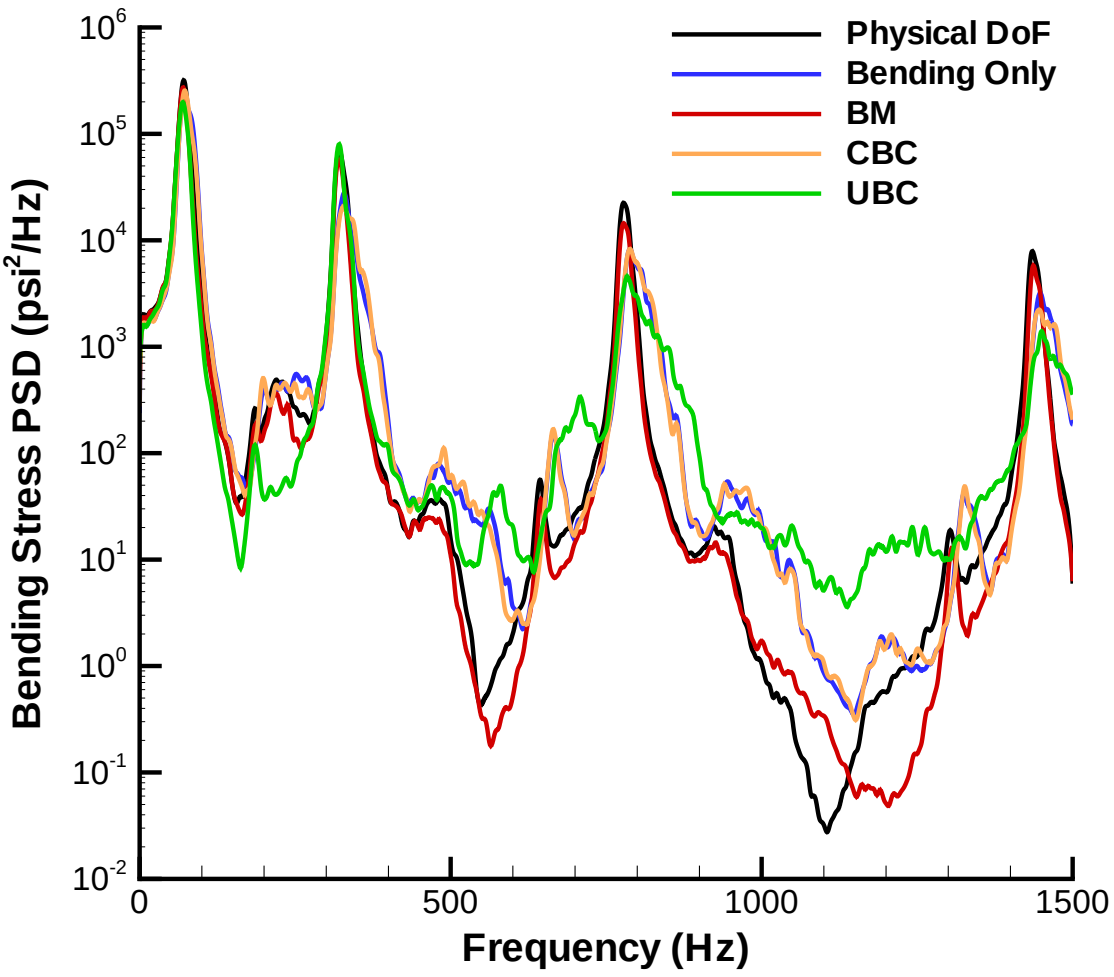

Figure 19: Clamped end bending stress for 152 dB loading.

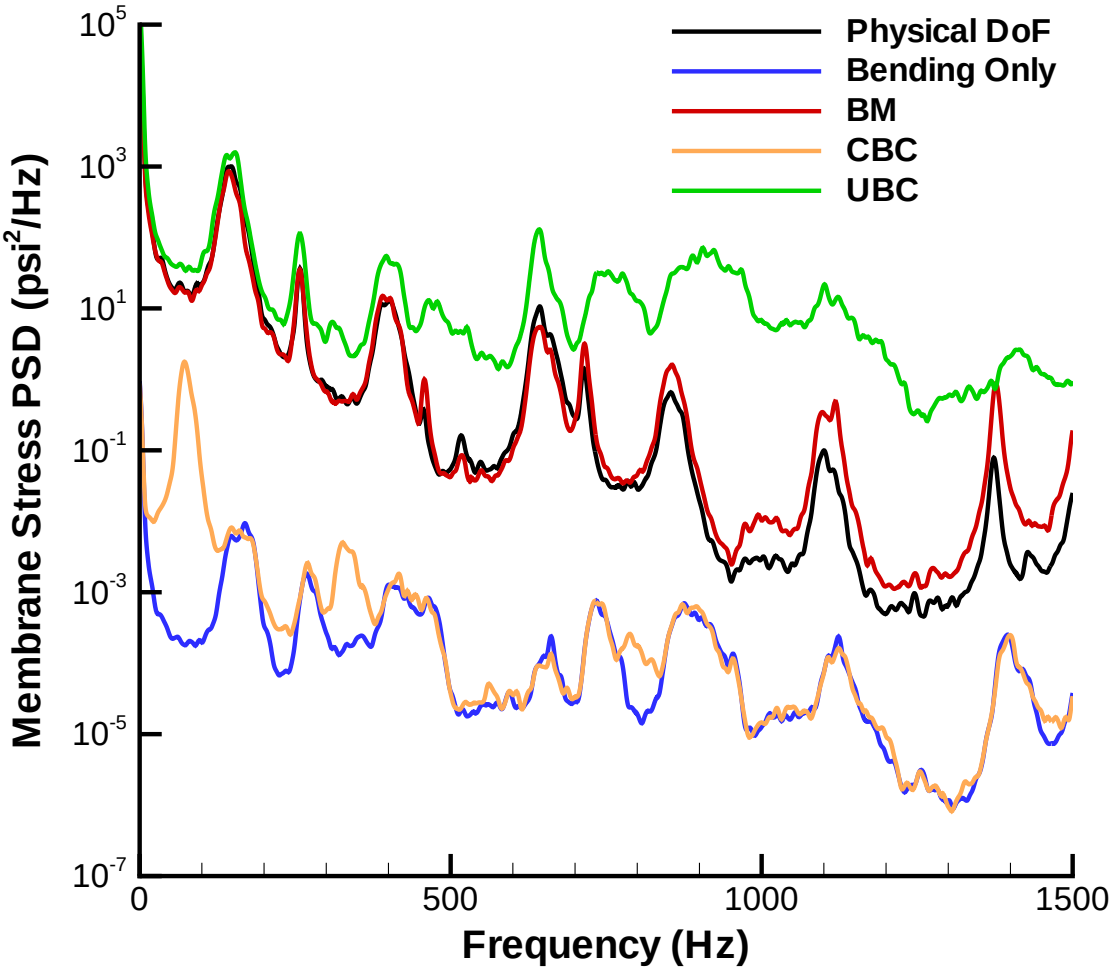

Figure 20: Clamped end membrane stress for 152 dB loading.

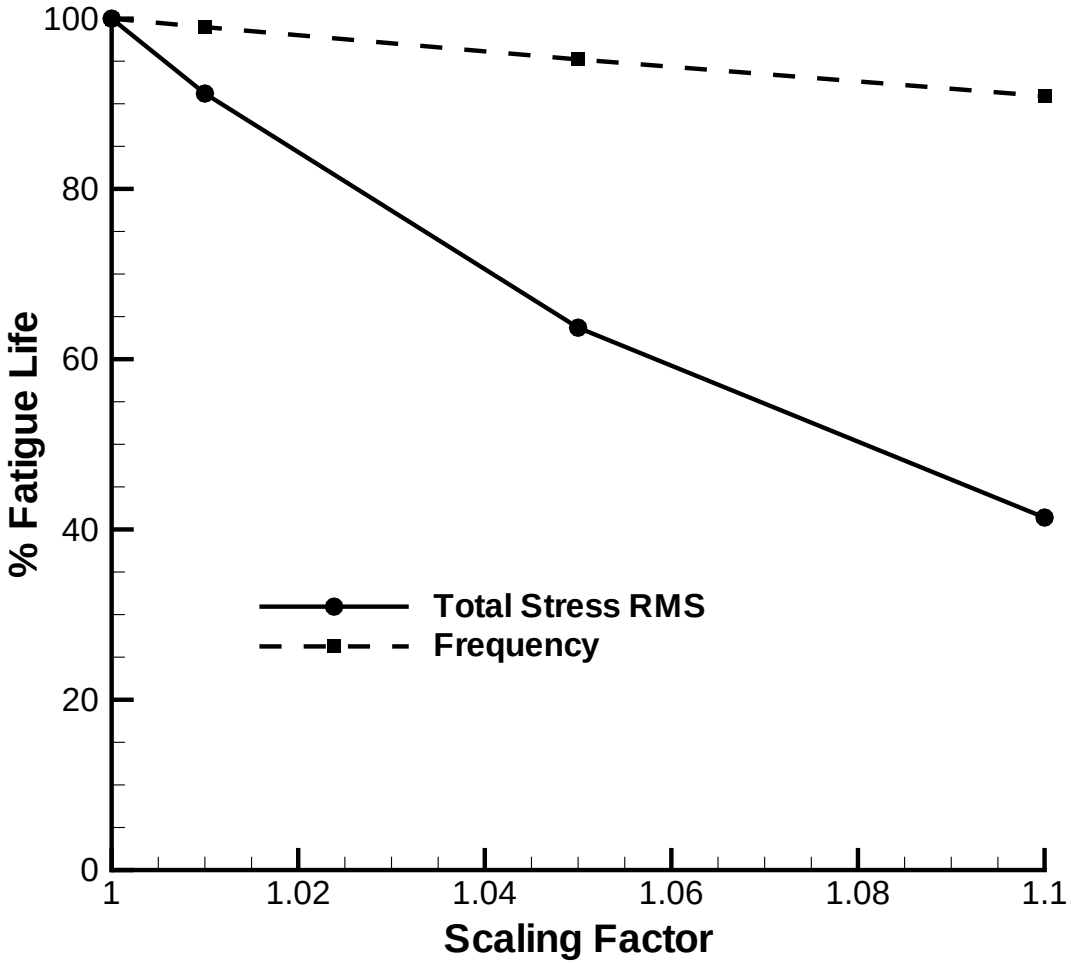

Figure 21: Sensitivity of fatigue life to changes in stress magnitude and frequency.

TABLE CAPTIONS

Table 1: Fatigue life estimates corresponding to the stress 90% confidence intervals ($R = -1$).

Table 2: Mean values of total stress (psi).

Table 3: Standard deviations of total stress (psi).

Table 4: Clamped end fatigue life estimates at 152 dB using calculated stress ratios.

Table 1: Fatigue life estimates corresponding to the stress 90% confidence intervals ($R = -1$).

Location	OASPL (dB)	Units	Physical DoFs	B 6	BM 6+6	CBC 6	UBC 6+4
Clamped End	146	Years	247.0–771.7	304.1–752.7	392.8–1300.4	312.5–771.6	1080.4–2762.5
	152	Years	0.438–1.884	1.327–2.939	1.094–3.723	1.492–3.715	6.276–12.781
	164	Min.	1.554–4.214	1.478–3.764	4.351–15.403	2.746–7.219	n/a
Quarter-Span	146	Years ($x10^7$)	1.330–3.355	2.655–6.048	2.731–6.863	2.589–6.390	1.506–3.502
	152	Years ($x10^4$)	1.500–6.318	4.858–11.48	2.465–10.40	7.248–15.71	0.798–2.411
	164	Days	76.39–179.3	12.37–31.34	88.34–247.0	42.64–108.2	n/a

Table 2: Mean values of total stress (psi).

Location	OASPL (dB)	Physical DoFs	B	BM	CBC	UBC
Clamped End	146	69.03	0.60	67.59	-0.52	102.43
	152	210.26	2.99	194.01	-0.47	229.55
	164	1210.7	5.08	1170.3	7.26	n/s
Quarter-Span	146	68.74	121.48	69.87	121.78	18.28
	152	214.72	315.03	197.77	315.33	54.76
	164	1223.7	1689.9	1268.7	1695.1	n/a

Table 3: Standard deviations of total stress (psi).

Location	OASPL (dB)	Physical DoFs	B	BM	CBC	UBC
Clamped End	146	1378.8	1356.2	1332.2	1352.6	1286.0
	152	2685.0	2476.4	2466.0	2452.0	2256.1
	164	8751.3	8688.7	8234.9	8637.7	n/a
Quarter-Span	146	407.23	388.91	386.30	388.71	393.72
	152	867.72	756.64	814.66	739.99	838.67
	164	2985.9	2766.1	2950.9	2696.6	n/a

Table 4: Clamped end fatigue life estimates at 152 dB using calculated stress ratios. Asterisk indicates mean stress static correction applied.

	Physical DoFs	B	BM	CBC	UBC
Fatigue Life (years) / Stress Ratio (*R*)	3.526 / -0.73	8.639/ -0.72*	8.415/ -0.73	10.370/ -0.71*	68.415/ -0.66
	0.817 / -1.00	1.912 / -1.00	1.874 / -1.00	2.260 / -1.00	8.736 / -1.00